



HAL
open science

ILLUMINATING THE ALLOSTERIC MODULATION OF THE CALCIUM-SENSING RECEPTOR

Hongkang Liu, Ping Yi, Wenjing Zhao, Yuling Wu, Francine Acher,
Jean-Philippe Pin, Jianfeng Liu, Philippe Rondard

► **To cite this version:**

Hongkang Liu, Ping Yi, Wenjing Zhao, Yuling Wu, Francine Acher, et al.. Illuminating the allosteric modulation of the calcium-sensing receptor. *Proceedings of the National Academy of Sciences of the United States of America*, 2020, 117 (35), pp.21711-21722. 10.1073/pnas.1922231117 . hal-02933760

HAL Id: hal-02933760

<https://hal.science/hal-02933760>

Submitted on 17 Dec 2020

HAL is a multi-disciplinary open access archive for the deposit and dissemination of scientific research documents, whether they are published or not. The documents may come from teaching and research institutions in France or abroad, or from public or private research centers.

L'archive ouverte pluridisciplinaire **HAL**, est destinée au dépôt et à la diffusion de documents scientifiques de niveau recherche, publiés ou non, émanant des établissements d'enseignement et de recherche français ou étrangers, des laboratoires publics ou privés.

Classification: Biological Sciences / Pharmacology

Illuminating the allosteric activation of a nutrient G protein-coupled receptor

Hongkang Liu^{1,2}, Ping Yi¹, Wenjing Zhao¹, Yuling Wu¹, Francine Acher³, Jean-Philippe Pin^{2*},
Jianfeng Liu^{1*} and Philippe Rondard²

¹ Cellular Signaling laboratory, International Research Center for Sensory Biology and Technology of MOST, Key Laboratory of Molecular Biophysics of MOE, and College of Life Science and Technology, Huazhong University of Science and Technology, 430074 Wuhan, Hubei, China.

² Institut de Génomique Fonctionnelle (IGF), Université de Montpellier, CNRS, INSERM, 34094 Montpellier Cedex 5, France.

³ Faculté des Sciences Fondamentales et Biomédicales, CNRS, Université de Paris, 75270 Paris Cedex 6, France.

* Correspondence to:

Jean-Philippe Pin, Institut de Génomique Fonctionnelle, 141 rue de la Cardonille, 34094 Montpellier, France. Email: jean-philippe.pin@igf.cnrs.fr; Tel: +33 434 35 9289.

or

Jianfeng Liu, Cellular Signaling laboratory, International Research Center for Sensory Biology and Technology of MOST, Key Laboratory of Molecular Biophysics of MOE, and College of Life Science and Technology, Huazhong University of Science and Technology, 430074 Wuhan, Hubei, China. Email: jfliu@mail.hust.edu.cn; Tel: +86-27-87792031.

Keywords

Signal transduction | allosteric modulator | calcium | amino acids | nutrient sensing

This PDF file includes:

Main Text

Figures 1 to 6

Supplementary Figures 1 to 11

Abstract

Many membrane receptors are regulated by nutrients. How these nutrients control a single receptor remains unknown, even in the case of the well-studied calcium-sensing receptor (CaSR) regulated by multiple factors including ions and amino acids. Here we developed an innovative cell-free FRET-based conformational CaSR biosensor to clarify the main conformational changes associated with activation. By allowing a perfect control of ambient nutrients, this assay revealed that Ca^{2+} alone fully stabilizes the active conformation, while amino acids behave as pure positive allosteric modulators. Based on the identification of Ca^{2+} activating sites, we propose a molecular basis for how these different ligands cooperate to control CaSR activation. Our results bring important information on CaSR function and for our understanding of the effects of genetic mutations responsible for human diseases. They also provide insights on how a receptor can integrate signals from various nutrients to better adapt the cell response.

Significance Statement

G protein-coupled receptors regulate many physiological processes and many of them sense nutrients. The mode of action of these nutrients remains elusive as it is difficult to control nutrient concentrations around living cells. The calcium-sensing receptor is regulated by multiple factors including ions and amino acids to control calcium homeostasis, and genetic mutations are responsible for human diseases. Here, we investigate this receptor in a perfect control of ambient nutrient. Based on the identification of calcium ions activating sites, we propose a molecular basis for how calcium and amino acids cooperate to control receptor activation. It leads to a novel model for the mechanism of activation of this receptor, and its modulation by multiple ligands and genetic mutations.

Main Text

Introduction

Cells have to constantly adapt to their environment, and as such sense through specific receptors a large number of nutrients, such as ions, L-amino acids (L-AAs), glucose, various metabolites and lipids (1). Despite the importance of such processes, how one receptor senses various nutrients remains elusive as it is difficult to control nutrient concentrations around living cells.

G protein-coupled receptors (GPCRs) form the largest family of membrane receptors and the major drug targets (2). Many of them are activated or modulated directly by nutrients (3, 4). Among GPCRs, the calcium-sensing receptor (CaSR) is a prototypical nutrients sensory receptor activated or modulated by both calcium (5) and amino acids (6), but also by endogenous and exogenous compounds such as different cations, polyamines, polypeptides and aminoglycoside antibiotics (7) (**Fig. 1A**).

The CaSR is essential in maintaining the extracellular calcium homeostasis. Indeed, CaSR is key in the negative loop that links calcemia and parathyroid hormone (PTH) secretion in the parathyroid gland (5). CaSR is also expressed in other tissues such as bone, gut, kidney and brain (5, 8), where it has additional effects. Many genetic mutations that lead to loss- or gain-of-function of the CaSR, have been identified in patients with metabolic syndromes, such as familial hypocalciuric hypercalcemia (FHH), neonatal severe primary hyperparathyroidism (NSPHT) or autosomal dominant hypocalcemia (ADH) (8, 9). In addition, CaSR autoantibodies that modify the signaling properties of the receptor have been identified in rare diseases (10). Finally, CaSR is the target of three commercial drugs acting as a positive allosteric modulator (PAM). Etelcalcetide (11, 12) that targets the extracellular domain is used for the treatment of secondary hyperparathyroidism after dialysis, while cinacalcet (13, 14) and

evocalcet (15) bind to the transmembrane domain and are used for the treatment of both primary and secondary hyperparathyroidism.

CaSR belongs to the class C GPCRs, and most of these receptors are activated by L-AAs or derivatives that bind to the conserved extracellular Venus flytrap (VFT) binding domain, such as the mGlu, GABA_B, GPCR6A and umami taste receptors, as well as the fish olfactory receptors and some pheromone receptors (16). These receptors form obligatory dimers providing a unique mode of activation compared to GPCRs from other classes. Like most class C GPCRs, each subunit of the CaSR homodimer is composed of an extracellular domain (ECD) made of a VFT and a cysteine-rich domain (CRD) connected to a heptahelical transmembrane domain (7TM) responsible for G protein coupling (**Fig. 1A**). Numerous studies have been performed to understand the molecular bases of calcium ions and amino acids actions on the CaSR (17). Recent crystal structures of the isolated ECD have been solved in absence or presence of calcium and amino acids by two different groups (18, 19) (**Fig. 1B**), but how binding of these nutrients in this domain triggers receptor activation remains elusive.

These solved CaSR structures led to a proposed rearrangement of the ECD dimer upon activation (18). This rearrangement is limited to the closure of both VFTs upon Ca²⁺ binding, without a major reorientation of the VFTs (**Fig. 1B**). This is in contrast to what has been observed with the closely related mGlu receptors, for which, the closure of the VFTs results in a major reorientation of the VFTs (20-23) (**Fig. 1B**). However, this CaSR model appears similar to what was observed with the distantly related GABA_B heterodimer (18) (**Fig. 1B**), but this needs to be firmly documented with the full-length CaSR.

CaSR structures also revealed in much details the L-AAs binding mode, but the Ca²⁺ sites involved in receptor activation still remain unclear, especially due to the limited resolution of the structures. The two studies reporting CaSR structures eventually did not propose the

same Ca^{2+} sites (**Supplementary Fig. 1A-B**). The molecular basis for L-AA activity was also difficult to characterize in functional studies using cell-based assays, due to the ambient concentrations of ions and other nutrients including L-AAs that are difficult to control tightly.

In this study, we have developed an innovative assay to clarify the conformational changes occurring during CaSR activation, and to investigate how nutrients control this activation. We have set up a time-resolved FRET (TR-FRET) conformational CaSR biosensor that enables to work in cell-free conditions, where the nutrients concentrations can be well-controlled (**Supplementary Fig. 2**). Using this assay, we demonstrate that calcium ions are sufficient to stabilize the active state of the receptor, while L-AAs have no effect on their own but enhance the effect of Ca^{2+} then acting as pure PAMs. Moreover, we show that chloride ions identified in the CaSR structures also act as PAMs, potentiating the effect of Ca^{2+} . We propose a model with two separate binding sites for calcium ions in each CaSR VFT, allowing an indirect interaction of both Ca^{2+} ions with the L-AA. Our data allowed us to understand the structural bases of the allosteric interaction between the calcium ions and the amino acids in the CaSR and then provide new insights on how nutrients can directly activate or allosterically regulate a membrane receptor.

Results

Development of a FRET-based conformational sensor for the CaSR

In order to better understand the mode of action of various ligands of the CaSR, we first aimed at clarifying the conformational changes associated with its activation, to see if it is similar to that of the mGluRs or of the GABA_B receptor. We used the same SNAP-tag and FRET-based approach as that used to examine conformational changes in mGlu and GABA_B receptors (20, 23). The CaSR subunit was fused at its N-terminus with a SNAP-tag that can be covalently labeled with time-resolved compatible fluorophores using specific cell-impermeant SNAP substrates (24) (**Fig. 1C**). In the absence of agonists, when the cells are incubated in a calcium free buffer, a high signal is measured between the two SNAP-tags of the CaSR dimer (**Fig. 1D**). Upon calcium addition, a large and fast decrease in FRET is measured, and the high FRET signal is restored with a calcium-free buffer (**Fig. 1D**). Accordingly, the FRET decay is slower in the presence of calcium (**Supplementary Fig. 3A**). Since the TR-FRET signal is mostly dependent on the distance between the donor and the acceptor, the strong decrease of FRET revealed a large increase in distance between the two N-terminal SNAP-tags, similar to that observed in mGluRs (20, 23), but different from what was observed with the GABA_B receptor for which a limited reorientation of the VFT occurs during activation (25).

To prove that the change of TR-FRET reflects receptor activation, we analyzed the effect of different CaSR agonists. They all consistently induced a decrease in FRET efficiency with potencies (fitted pEC₅₀) in the range of those measured using cellular functional assays: the inositol phosphate (IP₁) accumulation and intracellular calcium (Ca²⁺_i) assays (**Fig. 1E-H and Supplementary Fig. 3B-D**). Such a movement of the ECDs should also be affected by allosteric modulators acting in the 7TM domain (20), such as those developed for the CaSR (13) (**Supplementary Fig. 3E**). As expected, two commercial allosteric modulators of the CaSR, NPS R-568 (26) and NPS 2143 (27), that are positive and negative allosteric modulators,

respectively, were found to influence the agonist-induced changes in TR-FRET. While the NAM NPS2143 decreased agonist potencies, the PAM NPS R-568 enhanced agonist potencies in the TR-FRET assay (**Fig. 1I**). These data are perfectly in line with those obtained with the IP₁ functional assay (**Supplementary Fig. 3F**).

Altogether, our data show that the CaSR dimer undergoes a similar change in conformation at the level of the VFTs as that observed in mGluRs (20-23). This conformational change can be used to monitor the activation of the receptor, and to analyze the effects of ligand binding on the conformation of the receptor including allosteric modulation.

FRET sensor to detect the CaSR conformation stabilized by mutations

To further validate our sensor as a tool to measure the conformational change of the receptor, we have introduced mutations in regions of the receptor known to control the active state of receptor. We show that the A843E^{7,38} genetic and gain-of-function mutation (28) in the transmembrane domain 7 (TM7) that induced autosomal dominant hypocalcemia, stabilized the activate state of the ECD as revealed by the low FRET signal (**Fig. 1J**), without changing the cell surface expression of the receptor (**Supplementary Fig. 3G**). This is consistent with the reported constitutive activity of this mutant (28) (**Supplementary Fig. 3H**).

While the mechanism of activation of the mGluR ECD has been well-studied (21, 22, 29-31), less is known for the CaSR. Crystal structures of the isolated CaSR ECD revealed that the lower lobes of the VFT come closer in presence of agonists leading to a close contact between the CRDs (18). As reported with the mGlu2 receptor (32), the mutation of Pro569 into Cys led to a largely reduced FRET signal (**Fig. 1J**) despite a normal cell surface expression (**Supplementary Fig. 3G**). This mutation also induced a strong constitutive activity of the receptor in the IP₁ accumulation assay (**Supplementary Fig. 3H**), consistent with a stabilization of the receptor in an active state likely resulting from the crosslinking of the two

CRDs. These data are consistent with Pro569 being at the CRD interface in the active ECD structure of the CaSR (18). Of note, Ca^{2+} can still further decrease the FRET signal (**Fig. 1J**), an effect that may be due to a fraction of receptors not being crosslinked, or alternatively that crosslinking did not stabilize the receptor in its fully active state.

FRET sensor unravels the rearrangement of CaSR dimer interface during activation

We then used the FRET sensor to investigate the changes in the 7TM dimer interface during the activation of the CaSR using a disulfide cross-linking approach, as recently reported for the mGlu (21, 33) and the GABA_B (34) receptors (**Fig. 2A-B**). We speculated that locking the active state 7TM interface should result in a lower basal FRET, while locking the inactive interface should limit Ca^{2+} -induced FRET change (**Fig. 2C**). We have screened positions in TM4, TM5, TM6 and TM7 since these transmembrane helices were involved in the interface of other class C receptors (21, 33, 34). After copper phenanthroline (CuP) treatment to favor disulfide cross-linking between the introduced Cys residues, we observed a low FRET signal relative to control for six mutants in TM6 (I822C^{6.54}, P823C^{6.55}, A824C^{6.56}, A826C^{6.58}, S827C^{6.59} and T828C^{6.60}) (**Fig. 2C**), and not for other positions in TM6 and in the other TMs (**Fig. 2C and Supplementary Fig. 4A-B**). In contrast, for some mutants in TM4 and TM5 (V740C^{4.48}, I741C^{4.49}, Y744C^{4.52}, T745C^{4.53} and M771C^{5.38}), CuP treatment resulted in a decrease in the Ca^{2+} effect suggesting these mutations prevent the full rearrangement of the ECD dimer induced by the agonist, or alternatively, that a fraction of the receptors can no longer reach an active state (**Fig. 2C**). No such effect on the Ca^{2+} -induced signal is observed with other cysteine mutants in these TMs (**Supplementary Fig. 4A**) and in the TM6 and TM7 (**Fig. 2C and Supplementary Fig. 4B**). It indicated that TM4s and TM5s form the resting interface of the CaSR. All mutants were well expressed to the cell surface compared to the wild-type receptor (**Supplementary Fig. 4C-D**).

We have verified that both resting and active interfaces were cross-linked by blot analysis of the SNAP-CaSR subunits after their labeling at the cell surface with a cell-impermeant fluorophore (**Fig. 2D**), as previously performed for the mGlu2 receptor (33). The wild-type CaSR dimer is covalently linked by disulfide bridges between the two VFTs, involving two conserved cysteines (Cys129 and Cys131), but that are not required for receptor assembly and activity (35, 36). Then first, we have mutated these cysteines into alanine in a construct named CaSR^{CACA} (**Fig. 2A**). As expected, this construct migrated mostly as a monomer in nonreducing conditions, in contrast to WT CaSR that migrated as a dimer (**Fig. 2D**). We then analyzed whether Cys residues introduced in the TM could cross-link the CaSR^{CACA}. Efficiency of cross-linking between the two subunits induced by CuP was quantified by the change in the dimer signal to the total quantity of CaSR subunit detected on blots (**Fig. 2D**). The results revealed efficient cross-linking when Cys was introduced in TM4, 5 or 6. As a negative control, no such cross-linking was observed with the mutant V737C^{4,45} (**Supplementary Fig. 4E**), a site in TM4 which cannot be cross-linked in agreement with the FRET results (**Supplementary Fig. 4A**). These data show that TM4, 5 and 6 very likely constitute the CaSR dimer interface. Finally, we have confirmed that TM6 dimer interface corresponds to the active state as stabilizing this interface with a cysteine cross-linking at residues Ala824^{6,56} or Thr828^{6,60} leads to a constitutively active receptor (**Fig. 2E**).

Altogether, our results revealed a relative rearrangement between the two 7TMs during activation. While TM4-5 of each subunit face each other in the inactive state, a TM6-TM6 contact occurs in active state (**Fig. 2F and Supplementary Fig. 4F**). This movement is then similar to that proposed for other class C GPCRs (21, 33, 34), and is consistent with the inactive and active-like structures of mGlu5 (21).

Ambient L-amino acids are pure PAMs of the CaSR

Some L-AAs, especially aromatic ones, are known to regulate CaSR activity (6). The binding

site of the L-AAAs in the VFT domain was found to be equivalent to the glutamate binding site in mGluRs, as revealed by site-directed mutagenesis (37, 38) and the crystal structures of the CaSR VFT dimer (18, 19). However, the exact role of L-AAAs in the activation process of the CaSR remains elusive as the CaSR function has always been studied in cellular assays, then in the presence of an unknown concentration of various of L-AAAs (39). As illustrated here, L-Phe produced a modest PAM effect measured either with our FRET sensor (**Supplementary Fig. 5A**), or with functional assays (**Supplementary Fig. 5B-C**) in living cells, in agreement with previous reports (6, 18, 19).

To be able to perfectly control the ambient L-AA concentration, we established a cell free assay for the CaSR based on membranes containing our TR-FRET based sensor. The sensor is functional (**Fig. 3A-C**), although agonist potencies were slightly better in living cells compared to membranes (**Fig. 3C,E**). This may possibly result from a loss of bound L-AAAs in the CaSR during membrane preparations.

To completely remove any L-AA, membranes were dialyzed, and under such condition Ca^{2+} potency was significantly lower but yet it induced a full rearrangement of the ECD indicating that L-AAAs are not required for Ca^{2+} to fully activate CaSR (**Fig. 3D-E**). As expected, the addition of L-AAAs such as L-Phe restored the high CaCl_2 potency measured in cells (**Fig. 3D-E**). As control, D-Phe had no effect on both non-dialyzed and dialyzed membranes (**Supplementary Fig. 5D-E**), consistent with previous studies (6). As an additional control, NPS R-568 induced similar potency changes of CaCl_2 in non-dialyzed and dialyzed membranes consistent with the absence of ambient NPS R-568-like compound (**Supplementary Fig. 5D-E**).

We have then determined the effect of all 20 natural L-AAAs at 10 mM (except L-Tyr at 1 mM) on these dialyzed membranes (**Fig. 3F-G and Supplementary Fig. 6**). In the absence of calcium most L-AAAs did not induce a significant FRET decrease, except L-Cys (**Fig. 3F**

and Supplementary Fig. 6). We could not exclude that slight basal FRET change in presence of L-Cys, as well as L-Leu and L-Met might be due to fluorescent quenching or some effects unrelated to receptor conformation change (**Fig. 3F**). It shows that L-AAs have no intrinsic capacity in stabilizing the active state of the CaSR in the absence of calcium. However, most L-AAs have a significant PAM effect at 10 mM as revealed by the increased calcium potency, except L-Leu, L-Asp, L-Lys and L-Pro (**Fig. 3G**). The aromatic L-AAs have the strongest PAM effects, as previously reported (6). The potency of each L-AA, was determined in the presence of 5 mM CaCl₂ (**Fig. 3H and Supplementary Fig. 7**), at which concentration L-AAs show the maximum PAM effects. Aromatic L-AAs are the most potent with EC₅₀ ranging from less than 100 μM (L-Trp and L-Tyr), to less than 1 mM (L-Phe and L-His). Of note, the L-Trp derivative TNCA (L-1,2,3,4-tetrahydronorharman-3-carboxylic acid) observed in the CaSR structure (19) displays the highest potency among all L-AAs tested (**Fig. 3G-H and Supplementary Fig. 5F**). This high potency (less than 100 nM) likely explains why this compound was co-purified with the CaSR from HEK-293 cells (19). Other non-aromatic L-AAs displayed potencies from around 1 mM (L-Ala, L-Gln, L-Glu, L-Ile, L-Ser, L-Thr and L-Val) to more than 10 mM (**Supplementary Fig. 7**).

A genetic mutation shows a stronger PAM effect of L-AAs

Our FRET biosensor enables to investigate more precisely the molecular basis of genetic mutations on L-AA action on CaSR. As an example, we studied the genetic mutation E297D, responsible for the gain-of-function ADH (40). Glu297 is part of the L-AA binding site according to crystal structures (18, 19) and is proposed to be involved in Ca²⁺ binding (40-42). In the cellular format, Ca²⁺ has a higher potency for the mutant compared to WT (**Supplementary Fig. 8A,C**), while in dialyzed membranes, Ca²⁺ potency was similar on both receptors (**Supplementary Fig. 8B-C**). The high Ca²⁺ potency was recovered after addition of

L-Phe, with a more pronounced effect on the E297D mutant (**Supplementary Fig. 8B-C**). These data revealed that the gain-of-function of E297D mutation results from a more efficacious PAM effect of L-AAAs.

Chloride ions are PAMs at the CaSR

The structure of CaSR ECD in the active state (PDB 5FBK) (19) revealed three possible chloride binding sites (site *b*, *c* and *g*; **Fig. 4A**). As Cl⁻ ions were recently found to allosterically regulate most mGluRs (39, 43, 44), we investigated whether they could have any effect on the CaSR. We have performed TR-FRET assay in a gluconate buffer containing no chloride ions (“0 mM Cl⁻ buffer”, Cl⁻ being replaced by gluconate). In these conditions, calcium gluconate induced a large decrease in FRET indicating that Ca²⁺ was able to induce rearrangement of CaSR ECD in the absence of Cl⁻, although with a lower potency (**Fig. 4B, Supplementary Fig. 9A**). Chloride ions enhanced the Ca²⁺ effect by largely increasing its potency, while having no effect on their own, revealing a pure PAM action of Cl⁻ up to its physiological concentration (larger than 100 mM) (**Fig. 4B**). Similar results were obtained in intracellular calcium release assays (**Fig. 4C**).

Three chloride binding sites were reported in the VFT cleft (PDB 5FBK) (**Supplementary Fig. 9B-E**). Site *g* exists only in this structure but it is most probably a structural binding site for chloride, and as such was not studied further except through a mutation that has no effect (**Supplementary Fig. 9E**). Sites *b* and *c* are proposed to be a Ca²⁺ binding site in another active conformation of CaSR (PDB 5K5S) (**Supplementary Fig. 1**). Site *b* was also proposed to bind calcium in the resting state (PDB 5K5T). Site *b* is the most conserved Cl⁻ binding site in mGluRs (44) and other class C GPCRs such as the taste receptors T1Rs (PDB 5X2P) (45). Mutation of the most conserved residues of this site (**Supplementary Fig. 10**), T100A, impaired strongly the activation of the receptor by calcium. In contrast, the mutation T100E did not impair the activity of the receptor consistent with the distal carboxylate

group of Glu100 mimicking a chloride ion (44) (**Supplementary Fig. 9C**). These two mutations produced similar effect than the same mutations in mGlu4 receptor (44), suggesting this site could be a chloride binding site important for receptor function. In contrast, site *c* is composed of non-conserved residues (Arg66, Ser302 and Ser303) and their mutations do not strongly impair receptor activity (**Supplementary Fig. 9D**), suggesting this site is not important for chloride or calcium effects on CaSR.

Functional calcium binding sites nearby the L-AA at the CaSR

As already mentioned, several Ca^{2+} binding sites have been proposed based on the crystal structures of the CaSR dimer (18, 19), but none of them have been firmly validated, and discrepancies exist between the two studies (**Supplementary Fig. 1**).

The main Ca^{2+} site was proposed to be located between the lower lobes (lobes 2) in the VFT dimer interface, and other cations (magnesium, gadolinium) have been proposed to also bind at this interface (see sites *d-f*) (**Fig. 5A and Supplementary Fig. 1**) (18, 19, 46). It is a region composed of highly negatively charged residues with numerous Glu and Asp residues (**Fig. 5A and Supplementary Fig. 11A**) and reported to stabilize the active state of other class C GPCRs by binding cations that neutralize these negative repulsive electrostatic charges (47). We investigated the importance of this interface for calcium activation by site-directed mutagenesis. We have mutated all negative charges residues of this interface including residues shown to bind calcium, magnesium or even gadolinium in the CaSR structures (**Fig. 5A-B and Supplementary Fig. 11B-E**). These single and multiple mutants were well activated by calcium suggesting the activating binding site for calcium is not at this interface.

Among the other monatomic ion binding sites found in the crystal structures (**Supplementary Fig. 1**), sites *b* and *c* have low probability to bind functional Ca^{2+} as they likely bind Cl^- as shown above. In addition, site *a* is a conserved structural binding site for

cations as previously reported in mGluRs (48), and formed by the polypeptide backbone (**Supplementary Fig. 11F-G**), so it also has low probability to bind cations important for CaSR activation.

Since L-AAs have a strong PAM activity, and calcium was proposed to bind nearby the L-AA binding pocket in the receptor (19, 40, 41), we then explored this possibility for the Ca²⁺ binding site (**Fig. 5C**). The first possible site (site *I*, **Fig. 5D-E**) is located close to the hinge of the VFT. At this site, previous computational studies described a calcium ion binding to the conserved network of residues found in class C GPCRs activated by amino acids (e.g. mGluRs, DmXR, T1Rs, OR5.24, GPRC6A) (40, 46). This network makes a signature motif that interacts with the amino acid moiety of the various agonists (49) (**Supplementary Fig. 10**). However, none of the CaSR VFT crystal structures displays an ion at such a position. Instead, a water molecule is reported in the two crystal structures with enough resolution (5FBH and 5K5S) (18, 19). Changing this water molecule to a calcium ion and minimizing the binding residues, revealed the interactions previously computed with two different algorithms (Ser170, Asp190, Gln193, Tyr218, Glu297, **Fig. 5E**) (40, 46). Indeed, the electronic density radii of a calcium ion and oxygen of a water molecule are close (<http://abulafia.mt.ic.ac.uk/shannon/radius.php>). Accordingly, we were confident with site *I* and proceeded to its validation by mutagenesis and functional assays. Among the five mutants of the residues predicted to bind calcium, three (S170A, D190A and Y218A) largely impaired the Ca²⁺ effect (**Fig. 5F**) consistent with Silve *et al.* (40). Interestingly, the Hill number of Ca²⁺ on these mutants (S170A, $n_H = 1.44 \pm 0.18$; D190A, $n_H = 1.57 \pm 0.19$; and Y218A, $n_H = 1.09 \pm 0.19$) was much lower compared to that on the wild-type receptor ($n_H = 2.33 \pm 0.07$). It suggests one calcium ion binds in site *I*. Due to the dimeric nature of the CaSR, there are two sites *I* per receptor, then possibly explaining why the n_H is still higher than 1. Among the residues binding the calcium ion, Asp190 and Glu297 establish the strongest ionic interactions because of their negatively charged side chains. In

addition, Asp190 is found in the hinge of the VFT where the closing movement is initiated, and supporting its major role.

The highly cooperative nature of Ca^{2+} activation ($n_H > 2$) suggests the existence of at least a second site important for receptor activation (**Fig. 5G**). Zhang et al. have suggested that the electron density surrounded by Asp216, Ser272, Asp275 and a coordinating water molecule could be a magnesium ion (Mg^{2+}) (19). They finally opted for a highly ordered water molecule instead of a metal cation. Actually, a similar water molecule is found in all three structures of the closed CaSR VFT (PDB 5FBK, 5FBH and 5K5S) (18, 19). We propose that a calcium ion may be found in place of this water molecule, although this calcium binding site was not predicted in any of the previous computational studies. We made that change in the 3D-structure 5FBK and similarly in 5K5S. We observed interactions between calcium and Asp216, Ser272, Asp275 and a coordinating water molecule (**Fig. 5H**). In order to validate our model, we mutated these three residues to alanine in this site 2. Mutations D216A impaired strongly the activation of the receptor by calcium (**Fig. 5I**), and the Hill number is decreased ($n_H = 1.66 \pm 0.25$). It supports that one calcium ion could bind in this site 2. Finally, when the site 1 and 2 mutations were combined in the double mutant D190A-D216A (**Fig. 5J-L**), the receptor activation by Ca^{2+} was strongly impaired, in agreement with an additivity of the effect of these single mutants (**Fig. 5L**). We have verified that all the mutants were correctly expressed at the cell surface by ELISA (**Supplementary Fig. 11H**). Of note, we did not use the FRET CaSR biosensor to analyse calcium binding because the mutations *per se* already impaired the conformational equilibrium of the CaSR ECD.

Altogether, our results suggest there are two calcium binding sites in the L-AA binding pocket important for the activation of the receptor (**Fig. 6A-B**). In our model, both calcium ions are on each side of the L-AA and they interact indirectly with it (**Fig. 5E,H,K**). Ca^{2+} at site 1 interacts with L-AA through Ser170, Glu297 and Tyr218, while at site 2, calcium interacts with

L-AA through one water molecule. Consistent with a possible physiological role of these Ca^{2+} /L-AA interacting sites, a mixture of L-AAs at concentration found in fasting human brain plasma nicely potentiates Ca^{2+} -mediated responses in a physiological concentration range (**Fig. 6C**), but increasing the L-AA mix concentration, as observed after a protein-rich meal (50, 51), can further increase the effect of the physiological Ca^{2+} concentration (**Fig. 6D**).

Discussion

The CaSR is a prototypical nutrient receptor regulated by various signaling compounds including ions (Ca^{2+} and Mg^{2+} as activators, while SO_4^{2-} and PO_4^{3-} act as NAMs (18, 52)), L-AAs and polyamines like spermine (53). Structural studies also revealed CaSR can bind Cl^- . In the present study, we investigated how such structurally different compounds regulate this receptor. We first analyze the conformation changes associated with receptor activation at the level of the VFT, CRD and 7TM domains using a FRET based approach, and show strong similarity with mGluR activation, in contrast to previous models. This allowed us to validate a CaSR biosensor which was used to examine the action of various ligands in a cell-free and nutrients-controlled environment. We show that Ca^{2+} alone can fully stabilize the active state of the CaSR by inducing VFT closure and we identified two important sites for this effect. In contrast, most L-AA have no effect on their own but enhance Ca^{2+} potency at this receptor, acting then as pure PAMs, rather than co-agonists. We also revealed that chloride ions also act as PAMs of this important receptor.

As previously reported for mGluRs (20, 22, 23), we show that SNAP tag fusion at the N-terminus of the CaSR subunits allowed a direct analysis of the conformational change occurring during receptor activation. This can be recorded through TR-FRET measurements after covalent labeling of the subunits with SNAP substrates carrying compatible fluorophores. These data reveal a similar change in the VFT orientation of the CaSR compared to mGluRs upon activation (30) (**Fig. 6E**). This is in contrast to the proposed structures for the resting and active states of the CaSR (18), as the VFTs relative orientation is similar in both proposed states, corresponding to that observed in the active full-length mGlu5 structure (**Fig. 1B**). Then our data suggest a different conformation for the resting CaSR, likely closer to that observed with the resting mGluRs. Whatever, the CaSR active form predicted a close contact between the CRDs (18) that we validated by crosslinking experiments (**Fig. 6E**). Eventually, the sensor

was also helpful in identifying positions in the 7TM domain that can be crosslinked to lock the receptor either in the resting high FRET state, or the active low FRET state. Such analysis suggests a similar movement of the 7TM domains as previously reported for mGluR2 (33), or observed in the mGluR5 cryo-EM structures (21). Indeed, the TM4 and 5 of 7TM domains face each other in the resting state, while TM6 appears to be in close contact in the active state (**Fig. 6E**). Whether the 7TM domains contact each other in the inactive CaSR state is still questionable, as this is clearly not the case in the resting mGlu5 structure (21), although TM4 and 5 are indeed facing each other, allowing crosslinking to occur upon CuP treatment (33).

The use of the CaSR sensor allowed us to study its activation under controlled conditions, then either in the absence of Ca^{2+} , or in the absence of L-AA. This allowed us to demonstrate that Ca^{2+} alone was able to fully activate the receptor, while L-AAs at 10 mM cannot, indicating that L-AAs are pure PAMs. This is in apparent contrast to many class C GPCRs, including mGluRs, fish olfactory receptor such as zOlfCc1 (54) and OR5.24 (55), GPRC6A (56), the murine pheromone receptor mVmn2r1 (54) or the umami taste receptor (45) (including rat/mouse receptors) that can be directly activated by the L-AAs. This is even more surprising when one considers that the amino acid binding mode is very similar in all these receptors and involved the same residues interacting with the α -amino and α -carboxylic groups (49). However, we found that most L-AAs but Leu, Asp, Lys and Pro (at 10 mM), potentiate the effect of Ca^{2+} by increasing its potency, such that the active L-AA appears able to activate CaSR in the presence of low concentrations of Ca^{2+} . This raises the question whether some other class C GPCRs activated by L-AA also require Ca^{2+} for being activated. Indeed, many of these receptors are also regulated by Ca^{2+} (54, 56-58).

Structural studies revealed chloride ions bound to the CaSR VFT at three sites. Our data show that, as observed with mGluRs, Cl^- at physiological concentrations, is a PAM of the CaSR, an effect that involves two binding sites corresponding to those identified in mGluRs

(39, 44), further illustrating the similarity between these receptors. However, such an effect of chloride ions is unlikely to have any physiological effect, as their PAM effect is saturated at their physiological concentration, and it is not expected that plasma Cl^- concentrations will change sufficiently to affect CaSR activity.

Although calcium ions appear as the main and only direct activator of CaSR, it was surprising that its binding sites still remained elusive, despite the solved structures of the CaSR ECD by two groups (18, 19). Surprisingly, mutation of the Ca^{2+} sites proposed based on the structures, did not affect Ca^{2+} activation of the receptor, indicating that even though Ca^{2+} may bind at those sites, this does not affect the activity of the CaSR. Another possible Ca^{2+} site was previously predicted by modelling and docking studies in the L-AA binding pocket (40, 41, 59), called here site 1. The second site in this VFT binding pocket, site 2, was proposed to bind Mg^{2+} by the Yang's group (19). Our data nicely suggest that site 1 and site 2 are responsible for Ca^{2+} activation of CaSR. Mutating one of these sites resulted in a decreased Ca^{2+} effect, and most importantly, in a decreased n_{H} , from 2.3 for the WT to around 1.7 or below for the mutants, consistent with a decrease in the number of activating Ca^{2+} sites. The fact that the n_{H} remains significantly higher than 1 is also consistent with the dimeric nature of CaSR with a possible positive cooperativity between the subunits, as observed for the activation of mGluRs by glutamate (60). Of note, mutating both Ca^{2+} sites in each subunit result in a drastic decrease of Ca^{2+} activation, demonstrating the essential role of these two sites in CaSR activation. The low affinity of Ca^{2+} for these sites, plus the difficulty in assigning ions to specific densities in crystal structure (61) may explain why these two important sites have been missed when analyzing CaSR ECD structures.

All together, these data help us to propose a model for how Ca^{2+} and L-AA regulate CaSR activity. Ca^{2+} at site 1 interacts with residues close to the hinge region of the VFT, and contact residues from both lobes, then likely stabilizing the close active state of the VFT. Site

2 only involves residues from lobe 2 such that it is more difficult to imagine how Ca^{2+} binding at this site may be sufficient to activate the receptor, as observed when site 1 is mutated. It is possible that Ca^{2+} neutralizes negative charges such as that carried by D216, allowing the closure of the VFT, or that networks involving water molecules participate in stabilizing the closed VFT. Since L-AAs do not activate CaSR on their own, it is questionable whether they bind to the VFT in the absence of Ca^{2+} . However, because of the number of interactions they make with lobe 1 residues, we think they do. Possibly, they cannot stabilize the closed active VFT because of the repulsion of lobe 2 due to the negative charge of D216. Only when this charge is neutralized with Ca^{2+} bound at site 2 can the VFT close.

Taken together, our data clarify the mode of action of Ca^{2+} and L-AA on CaSR. The question of course remains whether the L-AA PAM effect is the result of the evolution of this receptor from L-AA activated class C GPCRs such as the mGlu, the fish L-AA olfactory or even the umami taste receptor, or whether such L-AA effect on CaSR is of physiological importance. Indeed, our well-controlled assay nicely confirms and further details that L-AA mix corresponding to that found in fasting human plasma can potentiate the effect of physiological concentrations of Ca^{2+} on the CaSR. Notably, increasing this L-AA mix concentration, as observed after a protein-rich meal, further potentiates the Ca^{2+} response. It is therefore likely that the increase in L-AA plasma concentration after a meal (up to 30 mM), enhances the Ca^{2+} effect leading to a decreased PTH secretion (6). Indeed, PTH plasma concentration is reduced after meal (50, 51). Whether this is only due to the allosteric control of CaSR by L-AAs or to other processes remains to be examined, but it is likely that this is at least playing a role. In conclusion, our data illustrate how a receptor could integrate the information coming from various structurally different nutrients to generate an optimized cellular response.

Materials and Methods

Materials

Calcium chloride, strontium chloride, magnesium chloride, spermine, neomycin, poly-L-arginine, poly-L-lysine, dichloro(1,10-phenanthroline)copper(II) (CuP), all the 20 common L-amino acids, D-phenylalanine, 4-(2-hydroxyethyl)-1-piperazineethanesulfonic acid (HEPES), lithium chloride, glucose, sodium carbonate, sodium gluconate, potassium gluconate, calcium gluconate, probenecid were purchased from Sigma-Aldrich (St. Louis, MO, USA). NPS R-568 was from Tocris Bioscience (Bristol, UK). NPS 2143 was from Abcam (Cambridge, UK). L-1,2,3,4-tetrahydronorharman-3-carboxylic acid (TNCA) was from Bachem (Bubendorf, Switzerland). Lipofectamine 2000 and Fluo4-AM were obtained from Thermo Fisher Scientific (Waltham, MA, USA). SNAP-Surface 649 was from New England Biolabs (Ipswich, MA, USA). SNAP-Lumi4-Tb, SNAP-Green labeling reagents and IP-One Gq kit were from Cisbio (Codolet, France).

Plasmids, transfection and cell surface quantification

The pRK5 plasmid encoding wild-type human CaSR, tagged with FLAG and SNAP inserted just after the signal peptide was subcloned from the pcDNA3 plasmid encoding CaSR (provided by Cisbio) to the pRK5 plasmid encoding mGluR2 as reported (20). All the mutants for CaSR were generated by site-directed mutagenesis using the QuikChange mutagenesis protocol (Agilent Technologies).

HEK293 cells (ATCC) and HEK293-TSA201 cells (ECACC) were cultured in DMEM (Thermo Fisher Scientific) supplemented with 10% fetal bovine serum (Sigma-Aldrich). For functional assays and cell surface expression quantification, HEK293 cells were transfected by electroporation 24 h before measurements (24). For FRET experiments, HEK293-TSA201

cells were transfected by Lipofectamine 2000 as previously described (24), 48 h before labeling to achieve high expression.

Detection of the CaSR expression at the cell surface was performed as previously described either by ELISA (23) or by fluorescent labeling (20).

Inositol phosphate (IP₁) accumulation measurements

IP₁ accumulation in HEK293 cells was measured using the IP-One Gq kit (Cisbio) according to the manufacturer's recommendations, except the stimulation buffer prepared separately (10 mM HEPES, 146 mM NaCl, 4.2 mM KCl, 1g/L glucose, 50 mM LiCl, pH adjusted to 7.4).

Intracellular calcium release measurements

Transfected HEK293 cells in black transparent flat-bottom 96-well plates were loaded with 1 μM Fluo4-AM in fresh buffer (130 mM NaCl, 5.1 mM KCl, 0.42 mM KH₂PO₄, 0.32 mM Na₂HPO₄, 5.27 mM glucose, 20 mM HEPES, 3.3 mM Na₂CO₃, 0.1% BSA, 2.5 mM probenecid, pH adjusted to 7.4) for 1 h at 37 °C. After a wash, cells were incubated with 50 μL buffer and 50 μL ligand solution at 2 × final concentrations were injected at 20 s during 60 s recording. Fluorescence signals (excitation 485 nm, emission 525 nm) were recorded by FlexStation 3 microplate reader or FLIPR Tetra (Molecular Devices, Sunnyvale, CA, USA) (24). To test chloride ions effects on CaSR, NaCl and KCl in the buffers were progressively replaced with gluconate equivalents (sodium gluconate and potassium gluconate, respectively) (44).

Cross-linking and fluorescent-labeled blot experiments

Cross-linking states of CaSR mutants were measured by fluorescent-labeled blot as previously described (33, 34). 48 h after transfection, adherent HEK293 cells plated in 12-well plates were labeled with 100 nM SNAP-Surface 649 in culture medium at 37 °C for 1 h. Cells were then washed once with PBS and cross-linked with 1.5 mM CuP in cross-linking buffer (16.7 mM

Tris, pH 8.0, 100 mM NaCl, 1 mM CaCl₂, 5 mM MgCl₂) at room temperature for 20 min. After incubation with 10 mM N-ethylmaleimide at 4 °C for 15 min to stop the cross-linking reaction, cells were lysed with lysis buffer (50 mM Tris, pH 7.4, 150 mM NaCl, 1% Nonidet P-40, 0.5% sodium deoxycholate) at 4 °C for 1 h. After centrifugation at 12000 g for 30 min at 4 °C, supernatants were mixed with loading buffer at 37 °C for 10 min. Equal amounts of proteins were resolved by 59:1 acrylamide:bisacrylamide and 6% SDS-PAGE. Proteins were transferred to nitrocellulose membranes (Millipore). Membranes were imaged by Odyssey CLx imager (LI-COR Bioscience, Lincoln, NE, USA).

FRET measurements for cells

Transfected HEK293-TSA201 cells in black non-transparent 96-well plates were labeled in FRET buffer (20 mM HEPES, 146 mM NaCl, 4.2 mM KCl, 1 g/L Glucose, 0.1% BSA, pH adjusted to 7.4) with 100 nM SNAP-Lumi4-Tb and 60 nM SNAP-Green at 37 °C for 1 h. Afterwards, cells were washed three times with FRET buffer, and drugs were added (to study effects of allosteric modulators NPS R-568 and NPS 2143, drugs were added 30 min before measurements). With excitation by a laser at 337 nm, the emission fluorescent intensities were recorded at 520 nm for two separate time windows (50-50 μs as window 1, 1200-1600 μs as windows 2) by PHERAstar FS microplate reader (BMG Labtech, Ortenberg, Germany) as described previously (20, 23). The FRET sensor values were determined by dividing the fluorescent intensities of window 1 by the intensities measured in window 2 (**Supplementary Fig. 3A**). Kinetic FRET measurements were performed with fluorescent intensities measured every 2 s during 90 s. To test chloride ions effects on CaSR, NaCl and KCl in the buffers were progressively replaced with gluconate equivalents (sodium gluconate and potassium gluconate, respectively) (44). For cross-linking experiments, cells were treated with 1.5 mM CuP in cross-linking buffer for 10 min (as described above for blot experiments) before labeling (33).

Preparation, dialysis, and FRET measurements for membranes

48 h after transfection and labeling in dishes, HEK293-TSA201 were washed three times, detached by Gibco enzyme-free cell dissociation buffer (Thermo Fisher Scientific) and collected by centrifugation at 1000 rpm for 5 min. Cells were resuspended in buffer (50 mM Tris, pH 7.4, 50 mM NaCl) with cOmplete protease inhibitor cocktail (Roche) and crushed through a 26 gauge 5/8 inch needle attached to a syringe for 25 passages. After centrifugation at 3000 rpm at 4 °C for 5 min, liquid supernatants were transferred to high-speed centrifuge tubes and centrifugated at 75000 rpm at 4 °C for 1 h by Optima MAX-TL ultracentrifuge (Beckman Coulter, Brea, CA, USA). The precipitated membranes were diluted gently in FRET buffer modified for membranes (20 mM HEPES, 146 mM NaCl, 4.2 mM KCl, pH adjusted to 7.4) and homogenized through a 26 gauge 5/8 inch needle for 15 passages. Membranes are dialyzed using Slide-A-Lyzer dialysis cassettes (MWCO 10000, Thermo Fisher Scientific) at 4 °C for 4 days in sterile membrane FRET buffer (changed with fresh ones every 24 h). Once prepared, non-dialyzed or dialyzed membranes are quantified with gradient dilution conditions using PHERAstar FS to recording emission fluorescent intensities (50-500 μ s) at 620 nm after excitation with a laser at 337 nm (23), and the working dilution condition is optimized. Then membranes are aliquoted, frozen quickly in liquid nitrogen and stored at -80 °C. For FRET measurements, membranes were thawed in membrane FRET buffer and plated in the 384-well plates. Ligand solutions at $2 \times$ final concentrations in same volume as the membrane solutions were added to wells 1 h before measurements. Same excitation and recording protocol as for cells in PHERAstar FS were used and the FRET sensor values are determined in the same way as for cells. Amino acids used for membranes were dissolved in the membrane FRET buffers with pH adjusted to 7.4 (L-Cys was prepared freshly before measurements). The L-AA mixtures mimicking the fasting conditions in plasma were prepared with the composition as previously reported (50 μ M L-Trp, 60 μ M L-Tyr, 50 μ M L-Phe, 80 μ M L-His, 300 μ M L-Ala,

250 μM L-Val, 75 μM L-Ile, 30 μM L-Met, 150 μM L-Leu, 125 μM L-Ser, 200 μM L-Thr, 50 μM L-Asn, 600 μM L-Gln, 30 μM L-Glu, 10 μM L-Asp, 100 μM L-Arg, 200 μM L-Lys, 30 μM L-Cys, 250 μM Gly and 180 μM L-Pro) (6).

Molecular modeling

Coordinates of CaSR VFTs were retrieved from the PDB (5K5S, 5K5T, 5FBH, 5FBK). Discovery Studio 2019 suite (Dassault Systèmes - BIOVIA, Vélizy-Villacoublay, France) was used for protein structure visualization and further computing. Minimizations were performed with the CHARMM forcefield applying the Smart Minimizer algorithm, (200 steps, generalized born with a simple switching -GBSW- implicit solvent and other default parameters). In all 3D models, proteins are shown as a solid ribbon, residue side chains and water molecules are displayed using the stick style and ions using the ball style, hydrogen atoms are not displayed for clarity.

Model of CaSR 7TM to show the residues substituted by cysteine (**Fig. 3B**) was retrieved from GPCRdb (62). Homology model of CaSR 7TM dimer in the active state was generated with Modeller 9.21 (63) based on the crystal structure of the dimeric mGluR5 (PDB 6N51) (21) using the loop optimization method. From the 100 models generated, the top ten classified by DOPE score were visually inspected, and the best scored structure with suitable loops was chosen in a position compatible with the cross-linking results (33).

Multiple sequence alignment analysis of ion binding sites was performed with Clustal Omega (64).

Curve fitting and data analysis

All data in figures and supplementary figures are mean \pm SEM of at least three independent experiments performed in triplicates unless stated separately in figure legends. Curves were fitted using linear regression (for correlation curves) or nonlinear regression (equation

“log(agonist) vs. response -- variable slope” for dose-response curves) in Prism software (GraphPad Software, San Diego, CA, USA). Intracellular calcium release data for ion binding sites (**Fig. 5B,F,I,L and Supplementary Fig. 9C-E, 11B-E**) are normalized together. FRET data of **Fig 2C and Supplementary Fig. 4A-B** are normalized and analyzed together. Quantified dimer ratio change data of **Fig 2D and Supplementary Fig. 4E** are analyzed together (mutants are compared with CACA). Significances were determined using one-way ANOVA with Dunnett’s multiple comparisons test (**Fig. 2D, 3F-G and Supplementary Fig. 4E**) or two-way ANOVA with Tukey’s multiple comparisons test (**Fig. 1J, 2C,E, 3E and Supplementary Fig. 3H, 4A-B, 5E, 8C**), with $P \leq 0.0001$ as ****, $P \leq 0.001$ as ***, $P \leq 0.01$ as **, $P \leq 0.05$ as *, $P > 0.05$ as ns.

Acknowledgments

We thank the Arpège platform in Institut de Génomique Fonctionnelle for providing facilities and technical support. We thank the Cisbio Bioassays for their support in providing reagents. J. L. was supported by the Ministry of Science and Technology of China (grant number 2018YFA0507003), the National Natural Science Foundation of China (NSFC) (grant numbers 31420103909, 81720108031, 31721002, and 81872945), the Program for Introducing Talents of Discipline to the Universities of the Ministry of Education (grant number B08029), and the Mériex Research Grants Program of the Institut Mériex. P. R. and J.-P. P. were supported by the Centre National de la Recherche Scientifique (CNRS), the Institut National de la Santé et de la Recherche Médicale (INSERM), and by grants from the Agence Nationale de la Recherche (ANR-09-BIOT-018-01), the FRM (Equipe DEQ20170336747). F.A. is supported by the Science Ambassador Program from Dassault Systèmes BIOVIA.

Author contributions

H.L., P.Y., J.-P.P., J.L. and P.R. designed experiments; H.L., P.Y., W.Z. and Y.W. performed molecular biology, cross-linking, FRET and functional assays; H.L., P.Y., J.-P.P., J.L. and P.R. performed data analysis; H.L. and F.A. performed molecular modelling; H.L., J.-P.P., J.L. and P.R. wrote the manuscript.

Competing interests

The authors declare no competing financial interests.

References

1. Efeyan A, Comb WC, & Sabatini DM (2015) Nutrient-sensing mechanisms and pathways. *Nature* 517(7534):302-310.
2. Hauser AS, Attwood MM, Rask-Andersen M, Schioth HB, & Gloriam DE (2017) Trends in GPCR drug discovery: new agents, targets and indications. *Nat Rev Drug Discov* 16(12):829-842.
3. Husted AS, Trauelsen M, Rudenko O, Hjorth SA, & Schwartz TW (2017) GPCR-Mediated Signaling of Metabolites. *Cell Metab* 25(4):777-796.
4. Zarzycka B, Zaidi SA, Roth BL, & Katriitch V (2019) Harnessing ion-binding sites for GPCR Pharmacology. *Pharmacol Rev* 71(4):571-595.
5. Brown EM & MacLeod RJ (2001) Extracellular calcium sensing and extracellular calcium signaling. *Physiol Rev* 81(1):239-297.
6. Conigrave AD, Quinn SJ, & Brown EM (2000) L-amino acid sensing by the extracellular Ca²⁺-sensing receptor. *Proc Natl Acad Sci U S A* 97(9):4814-4819.
7. Conigrave AD, Quinn SJ, & Brown EM (2000) Cooperative multi-modal sensing and therapeutic implications of the extracellular Ca²⁺ sensing receptor. *Trends Pharmacol Sci* 21(10):401-407.
8. Hannan FM, Kallay E, Chang W, Brandi ML, & Thakker RV (2018) The calcium-sensing receptor in physiology and in calcitropic and noncalcitropic diseases. *Nat Rev Endocrinol* 15(1):33-51.
9. Hu J & Spiegel AM (2003) Naturally occurring mutations of the extracellular Ca²⁺-sensing receptor: implications for its structure and function. *Trends Endocrinol Metab* 14(6):282-288.
10. Makita N, *et al.* (2019) Cinacalcet corrects biased allosteric modulation of CaSR by AHH autoantibody. *JCI Insight* 4(8).
11. Walter S, *et al.* (2013) Pharmacology of AMG 416 (Velcalcetide), a novel peptide agonist of the calcium-sensing receptor, for the treatment of secondary hyperparathyroidism in hemodialysis patients. *J Pharmacol Exp Ther* 346(2):229-240.
12. Alexander ST, *et al.* (2015) Critical Cysteine Residues in both the calcium-sensing receptor and the allosteric activator AMG 416 Underlie the Mechanism of Action. *Mol Pharmacol* 88(5):853-865.
13. Leach K, *et al.* (2016) Towards a structural understanding of allosteric drugs at the human calcium-sensing receptor. *Cell Res* 26(5):574-592.
14. Nemeth EF, *et al.* (2004) Pharmacodynamics of the type II calcimimetic compound cinacalcet HCl. *J Pharmacol Exp Ther* 308(2):627-635.
15. Kawata T, *et al.* (2018) A novel calcimimetic agent, evocalcet (MT-4580/KHK7580), suppresses the parathyroid cell function with little effect on the gastrointestinal tract or CYP isozymes in vivo and in vitro. *PLoS One* 13(4):e0195316.
16. Kniazeff J, Prezeau L, Rondard P, Pin JP, & Goudet C (2011) Dimers and beyond: The functional puzzles of class C GPCRs. *Pharmacol Ther* 130(1):9-25.
17. Zhang C, *et al.* (2016) Molecular Basis of the Extracellular Ligands Mediated Signaling by the Calcium Sensing Receptor. *Front Physiol* 7:441.
18. Geng Y, *et al.* (2016) Structural mechanism of ligand activation in human calcium-sensing receptor. *Elife* 5.
19. Zhang C, *et al.* (2016) Structural basis for regulation of human calcium-sensing receptor by magnesium ions and an unexpected tryptophan derivative co-agonist. *Sci Adv* 2(5):e1600241.

20. Doumazane E, *et al.* (2013) Illuminating the activation mechanisms and allosteric properties of metabotropic glutamate receptors. *Proc Natl Acad Sci U S A* 110(15):E1416-1425.
21. Koehl A, *et al.* (2019) Structural insights into the activation of metabotropic glutamate receptors. *Nature* 566(7742):79-84.
22. Levitz J, *et al.* (2016) Mechanism of Assembly and Cooperativity of Homomeric and Heteromeric Metabotropic Glutamate Receptors. *Neuron* 92(1):143-159.
23. Scholler P, *et al.* (2017) HTS-compatible FRET-based conformational sensors clarify membrane receptor activation. *Nat Chem Biol* 13(4):372-380.
24. Doumazane E, *et al.* (2011) A new approach to analyze cell surface protein complexes reveals specific heterodimeric metabotropic glutamate receptors. *FASEB J* 25(1):66-77.
25. Lecat-Guillet N, *et al.* (2017) FRET-Based Sensors Unravel Activation and Allosteric Modulation of the GABAB Receptor. *Cell Chem Biol* 24(3):360-370.
26. Nemeth EF, *et al.* (1998) Calcimimetics with potent and selective activity on the parathyroid calcium receptor. *Proc Natl Acad Sci U S A* 95(7):4040-4045.
27. Gowen M, *et al.* (2000) Antagonizing the parathyroid calcium receptor stimulates parathyroid hormone secretion and bone formation in osteopenic rats. *J Clin Invest* 105(11):1595-1604.
28. Zhao XM, Hauache O, Goldsmith PK, Collins R, & Spiegel AM (1999) A missense mutation in the seventh transmembrane domain constitutively activates the human Ca²⁺ receptor. *FEBS Lett* 448(1):180-184.
29. Muto T, Tsuchiya D, Morikawa K, & Jingami H (2007) Structures of the extracellular regions of the group II/III metabotropic glutamate receptors. *Proc Natl Acad Sci U S A* 104(10):3759-3764.
30. Rondard P & Pin JP (2015) Dynamics and modulation of metabotropic glutamate receptors. *Current opinion in pharmacology* 20:95-101.
31. Pin JP & Bettler B (2016) Organization and functions of mGlu and GABAB receptor complexes. *Nature* 540(7631):60-68.
32. Huang S, *et al.* (2011) Interdomain movements in metabotropic glutamate receptor activation. *Proc Natl Acad Sci U S A* 108(37):15480-15485.
33. Xue L, *et al.* (2015) Major ligand-induced rearrangement of the heptahelical domain interface in a GPCR dimer. *Nat Chem Biol* 11(2):134-140.
34. Xue L, *et al.* (2019) Rearrangement of the transmembrane domain interfaces associated with the activation of a GPCR hetero-oligomer. *Nat Commun* 10(1):2765.
35. Ray K, *et al.* (1999) Identification of the cysteine residues in the amino-terminal extracellular domain of the human Ca²⁺ receptor critical for dimerization. Implications for function of monomeric Ca²⁺ receptor. *J Biol Chem* 274(39):27642-27650.
36. Zhang Z, Sun S, Quinn SJ, Brown EM, & Bai M (2001) The extracellular calcium-sensing receptor dimerizes through multiple types of intermolecular interactions. *J Biol Chem* 276(7):5316-5322.
37. Mun HC, *et al.* (2004) The Venus Fly Trap domain of the extracellular Ca²⁺ -sensing receptor is required for L-amino acid sensing. *J Biol Chem* 279(50):51739-51744.
38. Zhang Z, *et al.* (2002) Three adjacent serines in the extracellular domains of the CaR are required for L-amino acid-mediated potentiation of receptor function. *J Biol Chem* 277(37):33727-33735.
39. Tora AS, *et al.* (2018) Chloride ions stabilize the glutamate-induced active state of the metabotropic glutamate receptor 3. *Neuropharmacology* 140:275-286.
40. Silve C, *et al.* (2005) Delineating a Ca²⁺ binding pocket within the venus flytrap module of the human calcium-sensing receptor. *J Biol Chem* 280(45):37917-37923.

41. Huang Y, *et al.* (2007) Identification and dissection of Ca²⁺-binding sites in the extracellular domain of Ca²⁺-sensing receptor. *J Biol Chem* 282(26):19000-19010.
42. Zhang C, *et al.* (2014) Direct determination of multiple ligand interactions with the extracellular domain of the calcium-sensing receptor. *J Biol Chem* 289(48):33529-33542.
43. DiRaddo JO, *et al.* (2015) Chloride is an agonist of group II and III metabotropic glutamate receptors. *Mol Pharmacol* 88(3):450-459.
44. Tora AS, *et al.* (2015) Allosteric modulation of metabotropic glutamate receptors by chloride ions. *FASEB J* 29(10):4174-4188.
45. Nuemket N, *et al.* (2017) Structural basis for perception of diverse chemical substances by T1r taste receptors. *Nat Commun* 8:15530.
46. Zhang C, *et al.* (2014) Identification of an L-phenylalanine binding site enhancing the cooperative responses of the calcium-sensing receptor to calcium. *J Biol Chem* 289(8):5296-5309.
47. Tsuchiya D, Kunishima N, Kamiya N, Jingami H, & Morikawa K (2002) Structural views of the ligand-binding cores of a metabotropic glutamate receptor complexed with an antagonist and both glutamate and Gd³⁺. *Proc Natl Acad Sci U S A* 99(5):2660-2665.
48. Kunishima N, *et al.* (2000) Structural basis of glutamate recognition by a dimeric metabotropic glutamate receptor. *Nature* 407(6807):971-977.
49. Acher FC & Bertrand HO (2005) Amino acid recognition by Venus flytrap domains is encoded in an 8-residue motif. *Biopolymers* 80(2-3):357-366.
50. Brown AJ, Koch MJ, & Coyne DW (2006) Oral feeding acutely down-regulates serum PTH in hemodialysis patients. *Nephron Clin Pract* 103(3):c106-113.
51. Sethi R, *et al.* (1983) Effect of meal on serum parathyroid hormone and calcitonin: possible role of secretin. *J Clin Endocrinol Metab* 56(3):549-552.
52. Centeno PP, *et al.* (2019) Phosphate acts directly on the calcium-sensing receptor to stimulate parathyroid hormone secretion. *Nat Commun* 10(1):4693.
53. Quinn SJ, *et al.* (1997) The Ca²⁺-sensing receptor: a target for polyamines. *Am J Physiol* 273(4):C1315-1323.
54. DeMaria S, *et al.* (2013) Role of a ubiquitously expressed receptor in the vertebrate olfactory system. *J Neurosci* 33(38):15235-15247.
55. Speca DJ, *et al.* (1999) Functional identification of a goldfish odorant receptor. *Neuron* 23(3):487-498.
56. Christiansen B, Hansen KB, Wellendorph P, & Brauner-Osborne H (2007) Pharmacological characterization of mouse GPRC6A, an L-alpha-amino-acid receptor modulated by divalent cations. *Br J Pharmacol* 150(6):798-807.
57. Tordoff MG, Alarcon LK, Valmeki S, & Jiang P (2012) T1R3: a human calcium taste receptor. *Sci Rep* 2:496.
58. Zou J, Jiang JY, & Yang JJ (2017) Molecular basis for modulation of metabotropic glutamate receptors and their drug actions by extracellular Ca²⁺. *Int J Mol Sci* 18(3).
59. Huang Y, *et al.* (2009) Multiple Ca²⁺-binding sites in the extracellular domain of the Ca²⁺-sensing receptor corresponding to cooperative Ca²⁺ response. *Biochemistry* 48(2):388-398.
60. Kniazeff J, *et al.* (2004) Closed state of both binding domains of homodimeric mGlu receptors is required for full activity. *Nat Struct Mol Biol* 11(8):706-713.
61. Echols N, *et al.* (2014) Automated identification of elemental ions in macromolecular crystal structures. *Acta Crystallogr D Biol Crystallogr* 70(Pt 4):1104-1114.
62. Pandey-Szekeres G, *et al.* (2018) GPCRdb in 2018: adding GPCR structure models and ligands. *Nucleic Acids Res* 46(D1):D440-D446.

63. Webb B & Sali A (2016) Comparative protein structure modeling using MODELLER. *Curr Protoc Protein Sci* 86:2 9 1-2 9 37.
64. Sievers F & Higgins DG (2018) Clustal Omega for making accurate alignments of many protein sequences. *Protein Sci* 27(1):135-145.

Figures

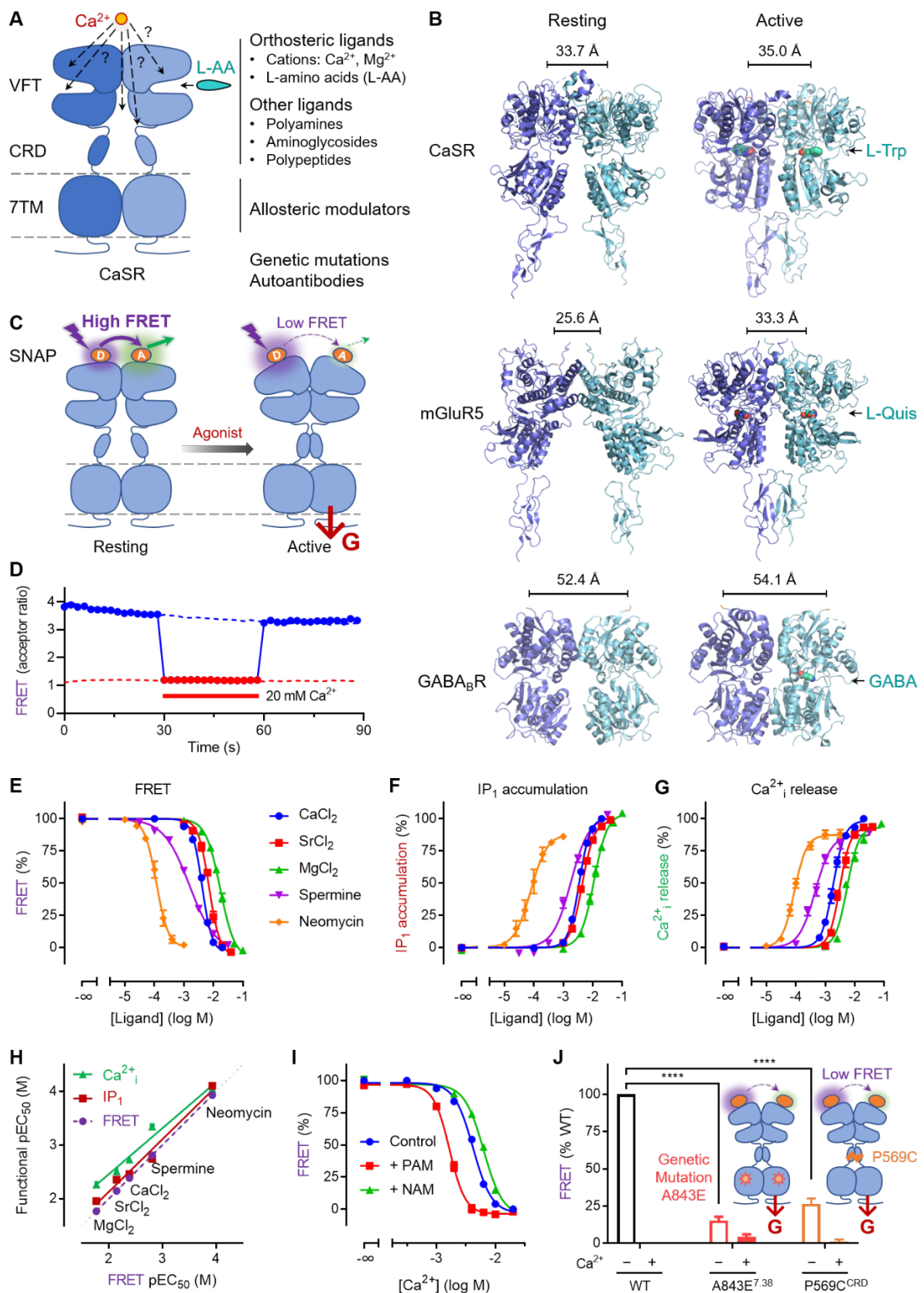


Figure 1. A conformational FRET-based sensor to investigate the structural dynamics of the CaSR ECD. (A) CaSR forms as a constitutive homodimer where each subunit (dark and

light blue, respectively) is composed of a large extracellular Venus flytrap domain (VFT) where L-AA binds, a cysteine-rich domain (CRD), a heptahelical transmembrane domain (7TM) responsible for allosteric modulators binding and an intracellular C-terminal region. Orthosteric binding sites for calcium remain unclear and controversial. Many genetic mutations have been found in patients with calcemic disorders, and they are located in the different regions of the receptor. Besides, autoantibodies have been identified in rare auto-immune diseases. **(B)** Crystal structures of the extracellular domain of class C GPCR dimers in the resting forms (left, CaSR PDB 5K5T biological assembly 2, mGluR5 PDB 6N52 and GABA_BR PDB 4MQE) and in the active forms in the presence of L-Trp, L-quisqualate or GABA (right, CaSR PDB 5K5S, mGluR5 PDB 6N51 and GABA_BR PDB 4MS3, respectively). **(C)** Cartoon illustrating the full-length SNAP-CaSR labeled with the Lumi4-Tb donor and the green fluorescent acceptor, with high FRET signal in the absence of agonist and a lower FRET signal in the presence of agonist. **(D)** FRET signal between the two VFTs after cell surface labeling of SNAP-CaSR expressing cells with fluorophores as indicated in panel C, in the presence of a saturating concentration of calcium (20 mM CaCl₂, injection at t = 30 s) and after calcium removal (t = 60-90 s). Data are mean ± SEM of a typical experiment performed in replicates. The control with 20 mM CaCl₂ (dotted red line) or buffer alone (dotted blue line) are shown for the same period of time (0-90 s). **(E-H)** Correlation (*H*) between the potencies (pEC₅₀) of different agonists on CaSR determined by FRET sensor assay (*E*), inositol monophosphate (IP₁) accumulation assay (*F*) and intracellular calcium (Ca²⁺_i) release assay (*G*). Data in panel *E-G* are mean ± SEM of at least three independent experiments performed in triplicates and normalized to the maximum response of CaCl₂. Data in panel *H* are mean ± SEM from the fitted curves for each individual experiment in panel *E-G*. **(I)** FRET signal measured for CaCl₂ in the presence of either PAM (10 μM NPS R-568) or NAM (10 μM NPS 2143). Data are mean ± SEM of at least three independent experiments performed in triplicates and normalized to the maximum response of the control. **(J)** FRET signal measured for the mutants A843E or P569C in the resting and active (20 mM CaCl₂) states (empty and filled, respectively). Data are mean ± SEM of at least three independent experiments performed in triplicates and normalized to WT. Data are analyzed using two-way ANOVA with Tukey's multiple comparisons test to determine significance, with **** *P* ≤ 0.0001.

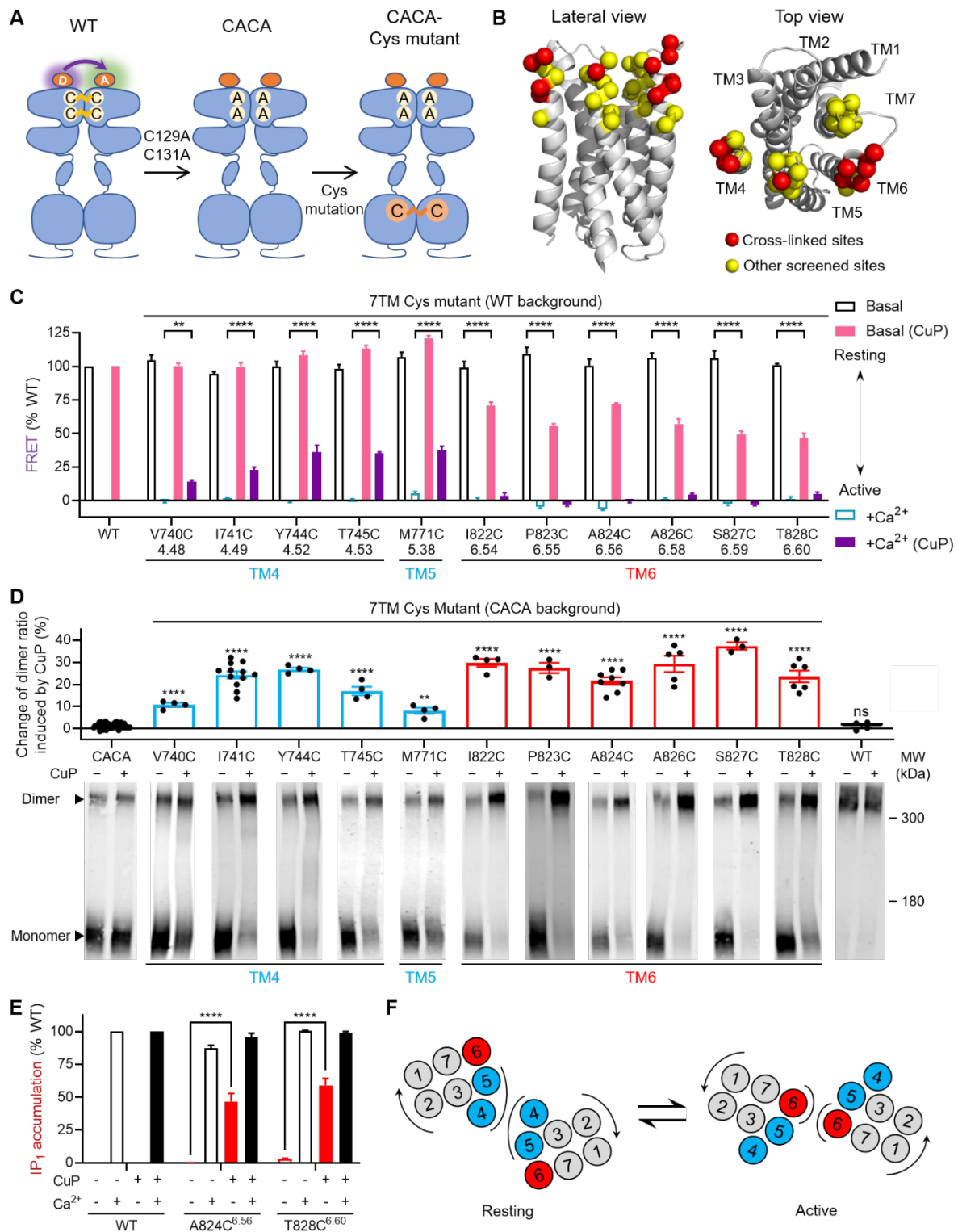


Figure 2. 7TM interface rearrangement is revealed by cysteine cross-linking and FRET. (A) Schematic representation of CaSR WT, mutant C129A-C131A (CACA, to remove the endogenous disulfide bonds between the two VFTs of CaSR dimer) and 7TM cysteine mutants with CACA background. (B) 3D model of the CaSR 7TM in lateral and top view. Residues substituted by cysteine are highlighted as yellow spheres (α carbon), and the well cross-linked ones are highlighted in red. (C) Cysteine cross-linked mutants screened by TR-FRET in the absence (black and pink) or presence of 20 mM CaCl₂ (blue and purple) with and without CuP treatment (filled and empty, respectively). Data are mean \pm SEM of at least three independent

experiments performed in triplicates and normalized to WT (data with and without CuP are normalized separately). Data are analyzed using two-way ANOVA with Tukey's multiple comparisons test to determine significance within each mutant group, with **** $P \leq 0.0001$ and ** $P \leq 0.01$. **(D)** Analysis of cell surface CaSR subunits of the cysteine mutants (CACA as control) in SDS-PAGE experiments under non-reducing conditions, after treatment (+) or without treatment (-) with CuP (lower panel). Changes of dimer ratio induced by CuP treatment for WT, the CACA control and every indicated mutant are quantified and shown (upper panel). Quantitative data are mean \pm SEM of at least four independent experiments (n = 4-12) while the blot for each mutant is representative of one of these experiments. Data are analyzed using one-way ANOVA with Dunnett's multiple comparisons test to determine significance (compared with CACA control), with **** $P \leq 0.0001$, ** $P \leq 0.01$ and ns $P > 0.05$. **(E)** IP₁ accumulation for WT and the indicated TM6 mutants after treatment (+) or without treatment (-) with CuP, in the absence or presence of 20 mM CaCl₂. Data are mean \pm SEM of at least three independent experiments performed in triplicates and normalized to WT (data with or without CuP are normalized separately). Two-way ANOVA with Tukey's multiple comparisons test within each mutant group, with **** $P \leq 0.0001$. **(F)** Model highlighting the TMs involved in the dimerization of CaSR in the resting state (TM4 and TM5, blue) and in the active state (TM6, red).

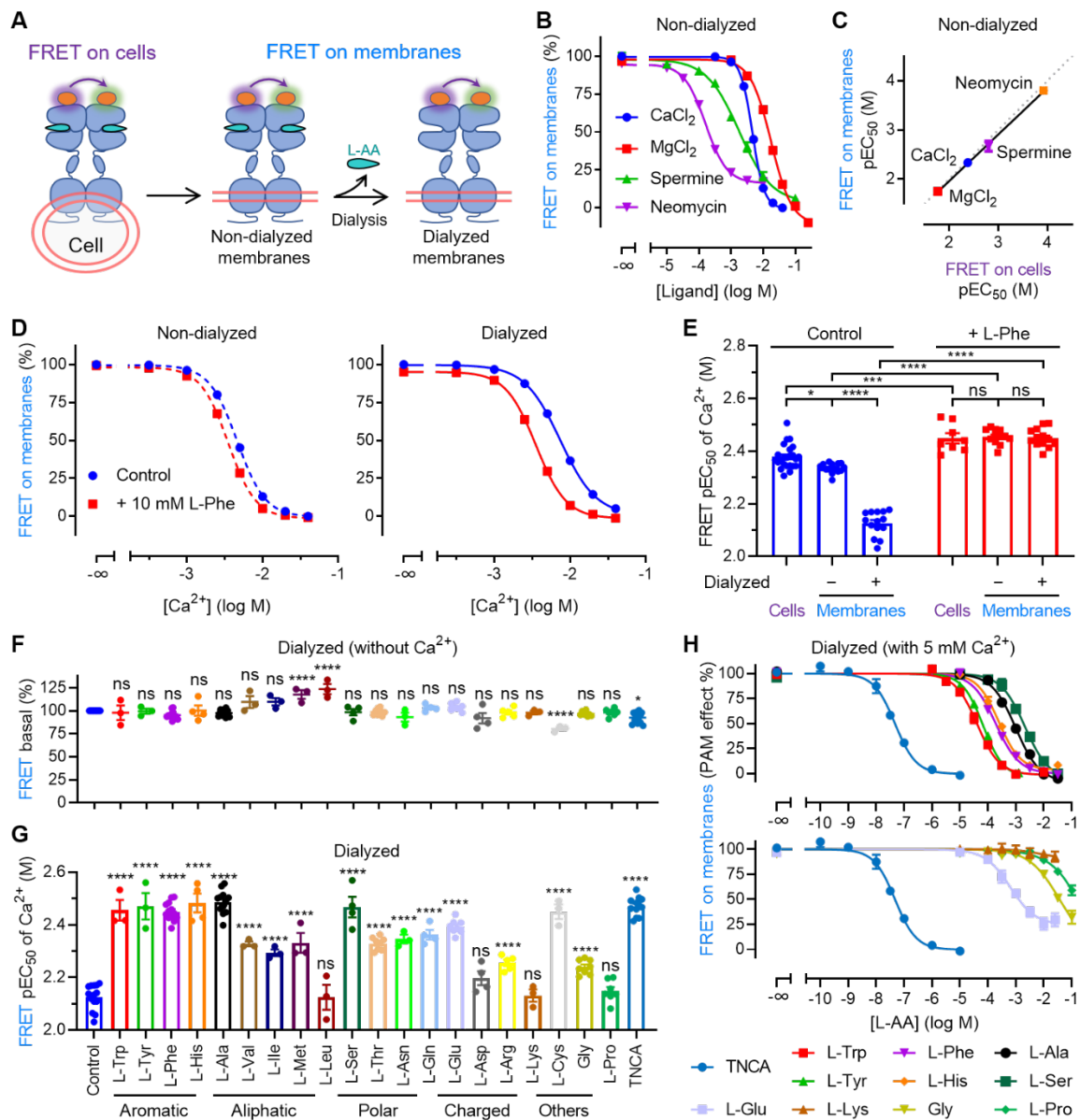


Figure 3. Allosteric modulation by L-AA is clarified with a cell-free assay. (A) Cartoon illustrating the development of FRET-based CaSR biosensor in a cell-free assay based on cellular membrane preparations as indicated. (B) FRET signal measured on non-dialyzed membranes with the indicated ligands. Data are mean \pm SEM of at least three independent experiments performed in triplicates and normalized to the maximum response of CaCl₂. (C) Correlation between the FRET potencies (pEC₅₀) of the indicated agonists determined on cells (X-axis) and non-dialyzed membranes (Y-axis). (D) FRET measurement performed with CaCl₂ on non-dialyzed (dotted lines) and dialyzed (solid lines) membranes in the absence (blue) or presence of 10 mM L-Phe (red). Data are mean \pm SEM of at least three independent experiments performed in triplicates and normalized to the basal of control and the maximum response of L-Phe (non-dialyzed and dialyzed data are normalized separately). (E) FRET potencies (pEC₅₀) of calcium on cells and on non-dialyzed (-) or dialyzed (+) membranes in the absence (blue) or presence of 10 mM L-Phe (red). Data are mean \pm SEM from at least eight independent experiments (n = 8-24). Two-way ANOVA with Tukey's multiple comparisons, with **** $P \leq 0.0001$, *** $P \leq 0.001$, * $P \leq 0.05$ and ns $P > 0.05$. (F) Basal FRET in the presence of the indicated L-AA at 10 mM (for Tyr 1 mM is used due to low solubility) or 10 μ M TNCA. Data are mean \pm SEM of at least three independent experiments (n= 3-13)

performed in triplicates and normalized to the control. One-way ANOVA with Dunnett's multiple comparisons test (compared with control) with **** $P \leq 0.0001$, * $P \leq 0.05$ and ns $P > 0.05$. **(G)** FRET potencies (pEC_{50}) of calcium on dialyzed membranes in the presence of the indicated amino acid (same concentrations as in panel *F*). Data are mean \pm SEM from at least three independent experiments ($n = 3-13$). One-way ANOVA with Dunnett's multiple comparisons test (compared with control) with **** $P \leq 0.0001$ and ns $P > 0.05$. **(H)** FRET signal change induced by the indicated L-AA performed on dialyzed membranes in the presence of 5 mM $CaCl_2$. Data are mean \pm SEM of at least three independent experiments performed in triplicates. Data are normalized to the basal conditions (5 mM $CaCl_2$ without L-AA) and the maximum response induced by L-AAs.

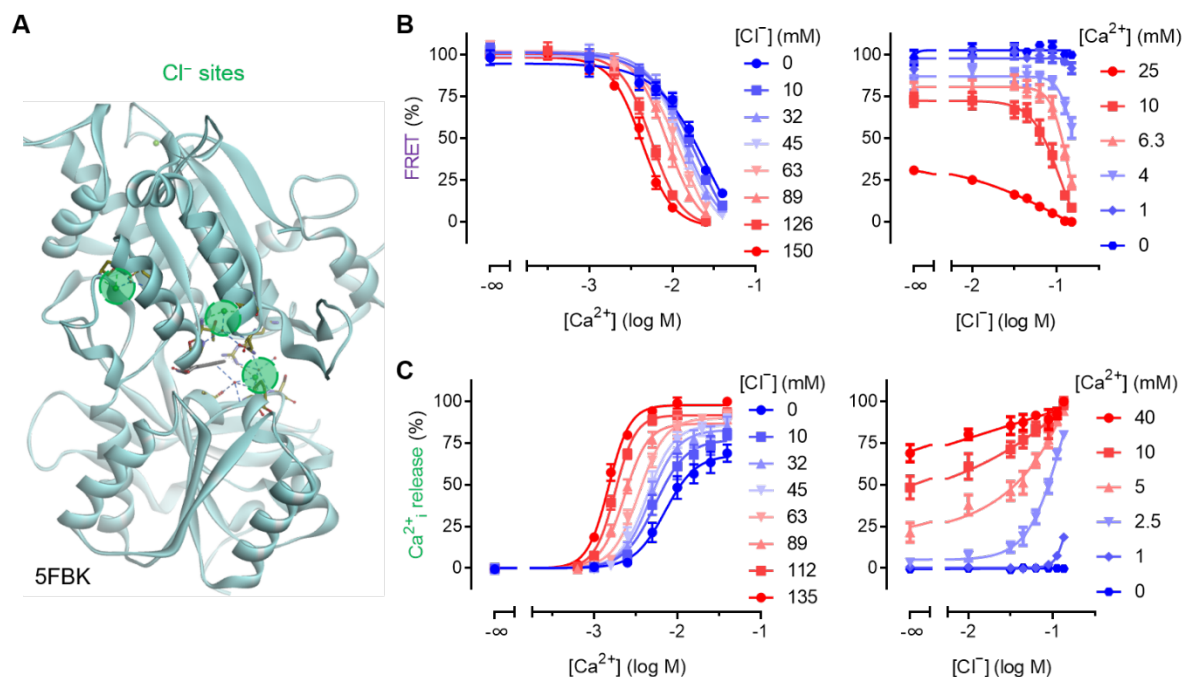


Figure 4. Allosteric modulation induced by chloride ions in CaSR VFT. (A) Three chloride binding sites were reported in the CaSR structure (PDB 5FBK). (B-C) FRET measurement (B) and intracellular calcium release (C) for calcium gluconate on CaSR performed in a buffer with the indicated concentrations of chloride ions. Either Ca²⁺ concentration (left) or Cl⁻ concentration (in buffer, right) is used as X-axis. Data are mean ± SEM of three independent experiments performed in triplicates and normalized to the maximum response in the buffer with the highest Cl⁻ concentration.

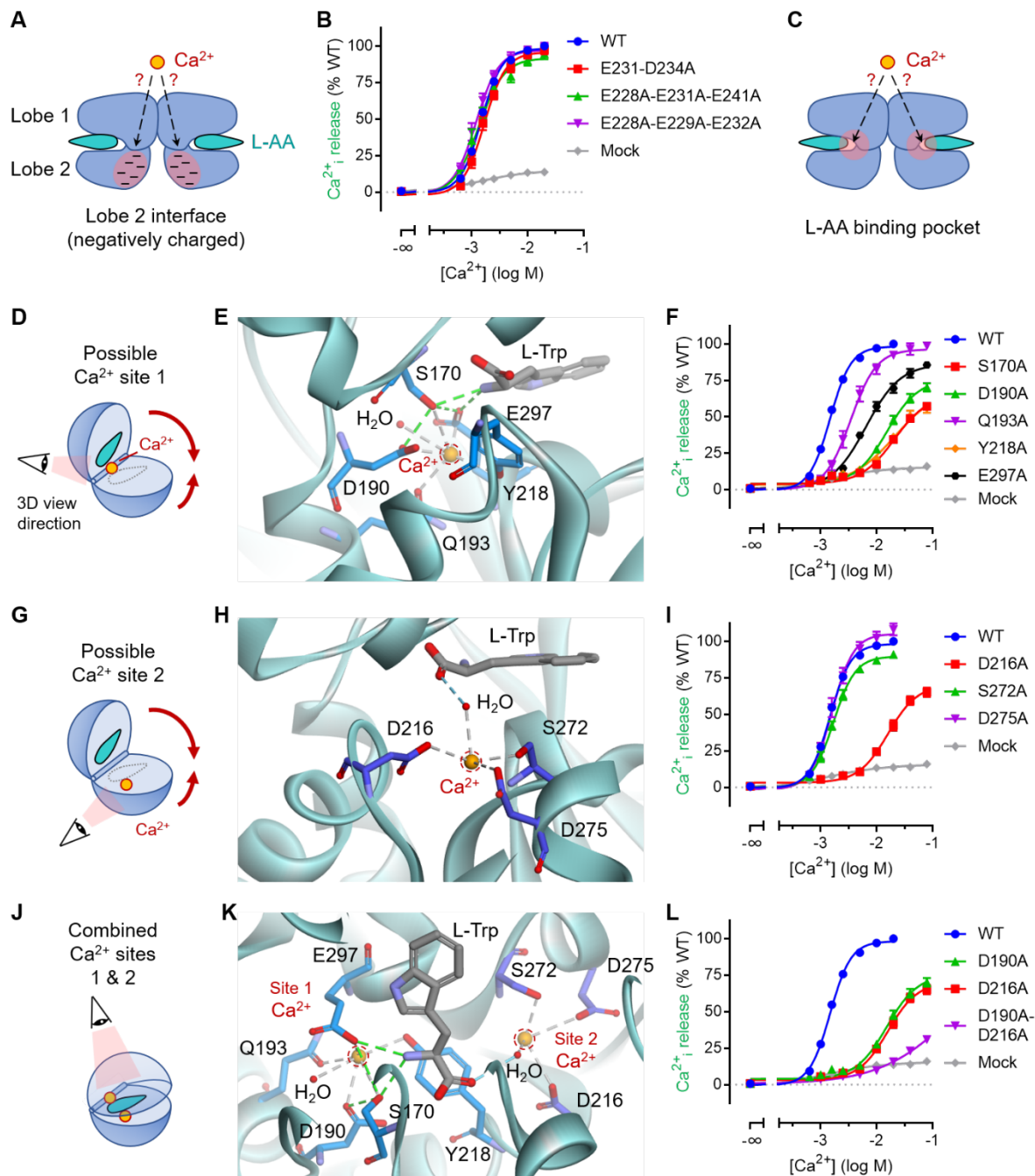


Figure 5. Binding of two calcium ions nearby L-AA stabilizes the active state. (A) Cartoon illustrating the possible calcium binding at the lobe 2 interface which was previously proposed to be important for receptor activation. (B) Intracellular calcium release for the indicated mutants in this lobe 2 interface. (C) Possible Ca^{2+} binding in the L-AA binding pocket. (d-f) Proposed Ca^{2+} binding *site 1* in the VFT hinge as illustrated by the cartoon (D), the 3D model of this site based on the crystal structure of the VFT (PDB 5K5S) (E) and intracellular calcium release data for the indicated mutant in this site (F). Ca^{2+} is proposed to be bound to S170, D190, Q193, Y218, E297 and one water molecule found in the crystal structure. (G-I) Similar analysis for the proposed calcium binding site 2 in the VFT adjacent to L-AA, and intracellular calcium release data for the indicated mutants. Ca^{2+} is proposed to be bound to the lobe 2 residues D216, S272, D275 and one water molecule found in the crystal structure (bridging this Ca^{2+} and bound L-Trp). (J-L) Combination of the two functional calcium binding sites *1* and *2* adjacent to the bound L-AA, top view of the L-AA surrounded by the two Ca^{2+} and

intracellular calcium release data for the indicated mutants. In the 3D model, interactions are shown as dashed lines (green for H-bonds, gray for metal bonds). Data in panel *B*, *F*, *I* and *L* are mean \pm SEM of at least three independent experiments performed in triplicates and normalized to WT.

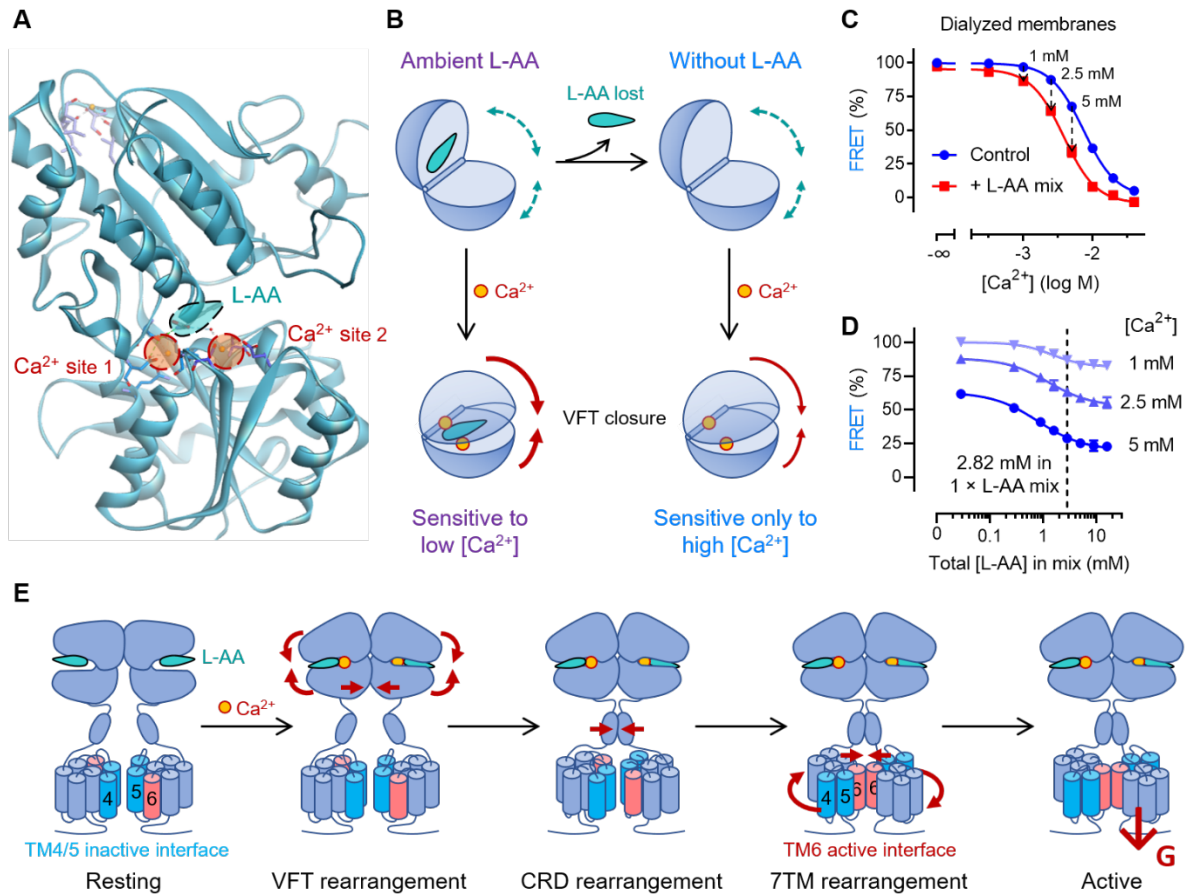
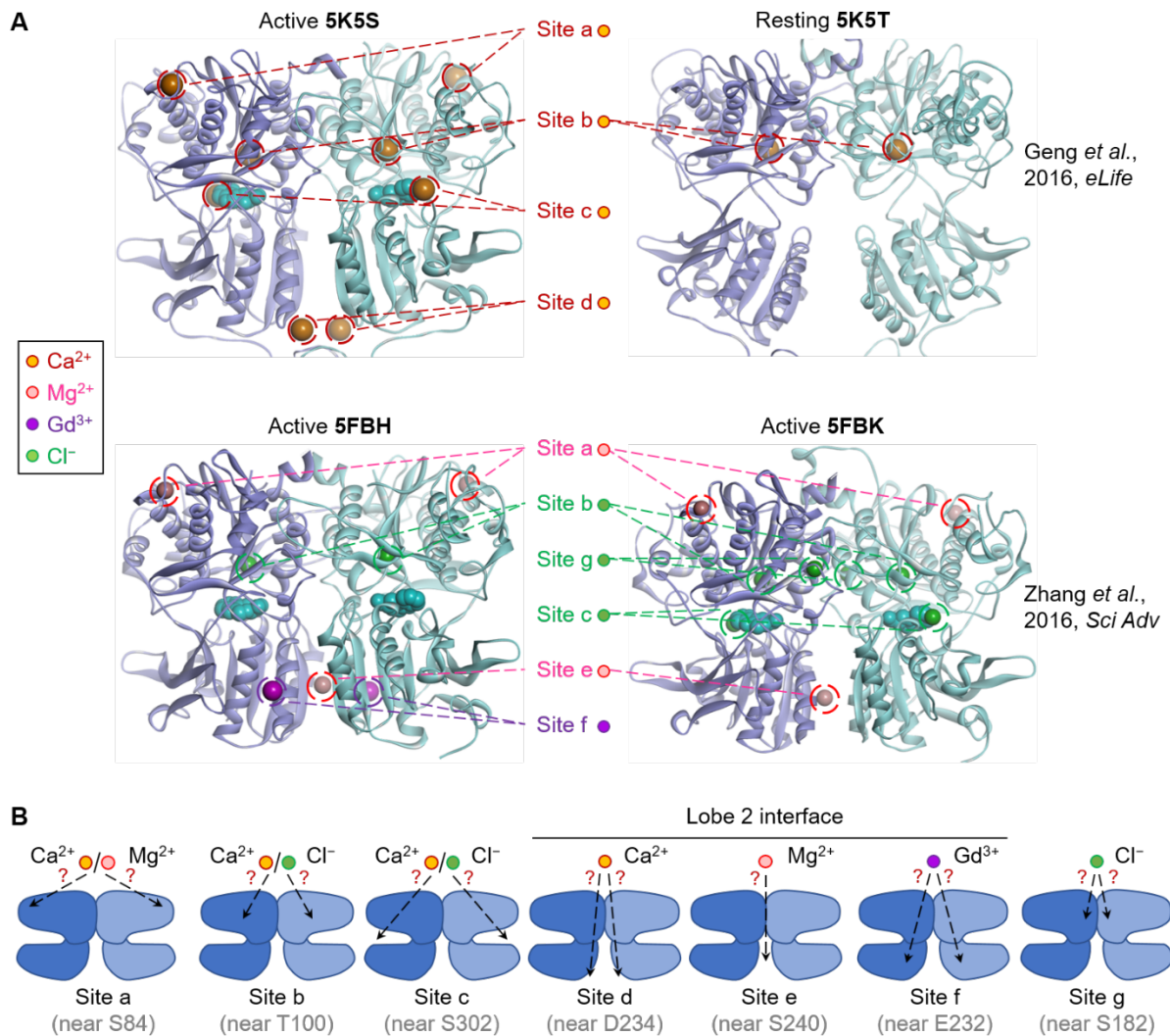
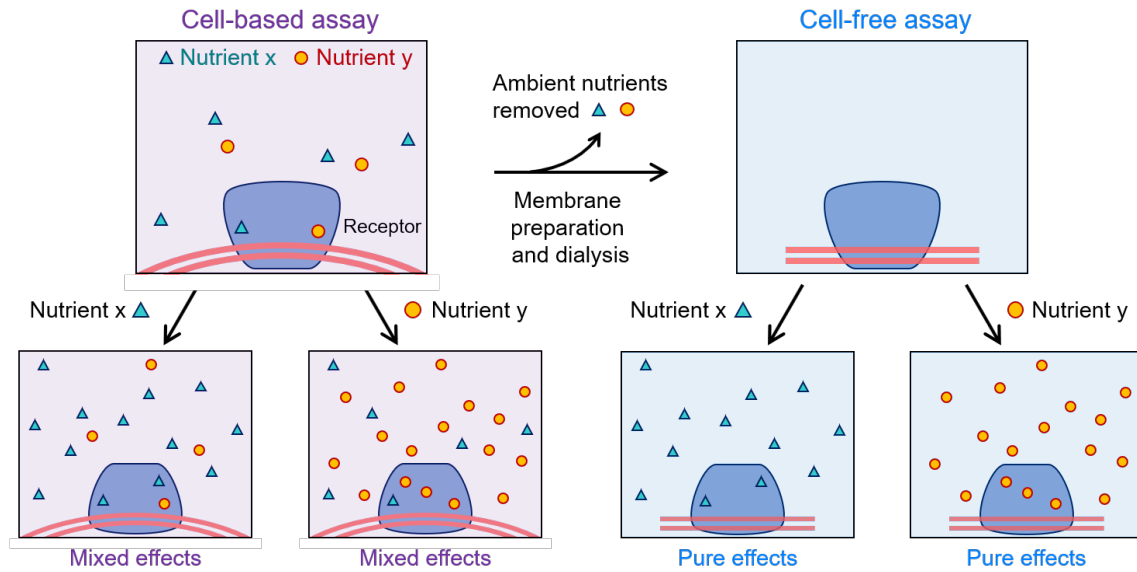


Figure 6. Model for the activation of CaSR. (A) 3D model of two possible functional calcium sites 1 and 2 near the bound L-AA based on the crystal structure of the VFT (PDB 5K5S). (B) VFT close state is proposed to be stabilized by calcium ions in the presence of ambient L-AA (cell-based conditions), but also by calcium ions alone in the absence of L-AA (cell-free conditions) during activation. The ambient L-AAs bound to CaSR VFT contribute to the high calcium potency and enable the receptor to sense low concentrations of calcium ions. But this high sensitivity to calcium is reduced when L-AA is lost. (C) FRET measurement performed with CaCl_2 on dialyzed membranes in the absence (blue) or presence of one-fold L-AA mixture (red). Data are mean \pm SEM of at least three independent experiments performed in triplicates and normalized to the basal of control and the maximum response of L-AA mixture. (D) FRET signal change induced by different folds of the L-AA mixture performed in dialyzed membranes in the presence of CaCl_2 . Data are mean \pm SEM of at least three independent experiments performed in triplicates. Data are normalized to the basal (without Ca^{2+} or L-AA) and the maximum response induced by Ca^{2+} in the presence of L-AA mixture. The vertical dotted line represents the related total concentration 2.82 mM of L-AAs used in one-fold L-AA mixture. (E) Molecular mechanism of activation of the CaSR upon L-AA and calcium binding. Binding of calcium ions in the VFT binding pocket most probably occupied by L-AA in physiological conditions, is expected to stabilize VFT closure and their relative rearrangement. Then it would induce CRD interactions and 7TM interface reorientation through allosteric propagation of the conformation changes. In the active state, TM6s will be at the dimer interface, a conformation required to stabilize at least one of the 7TM in the active state for G protein activation.

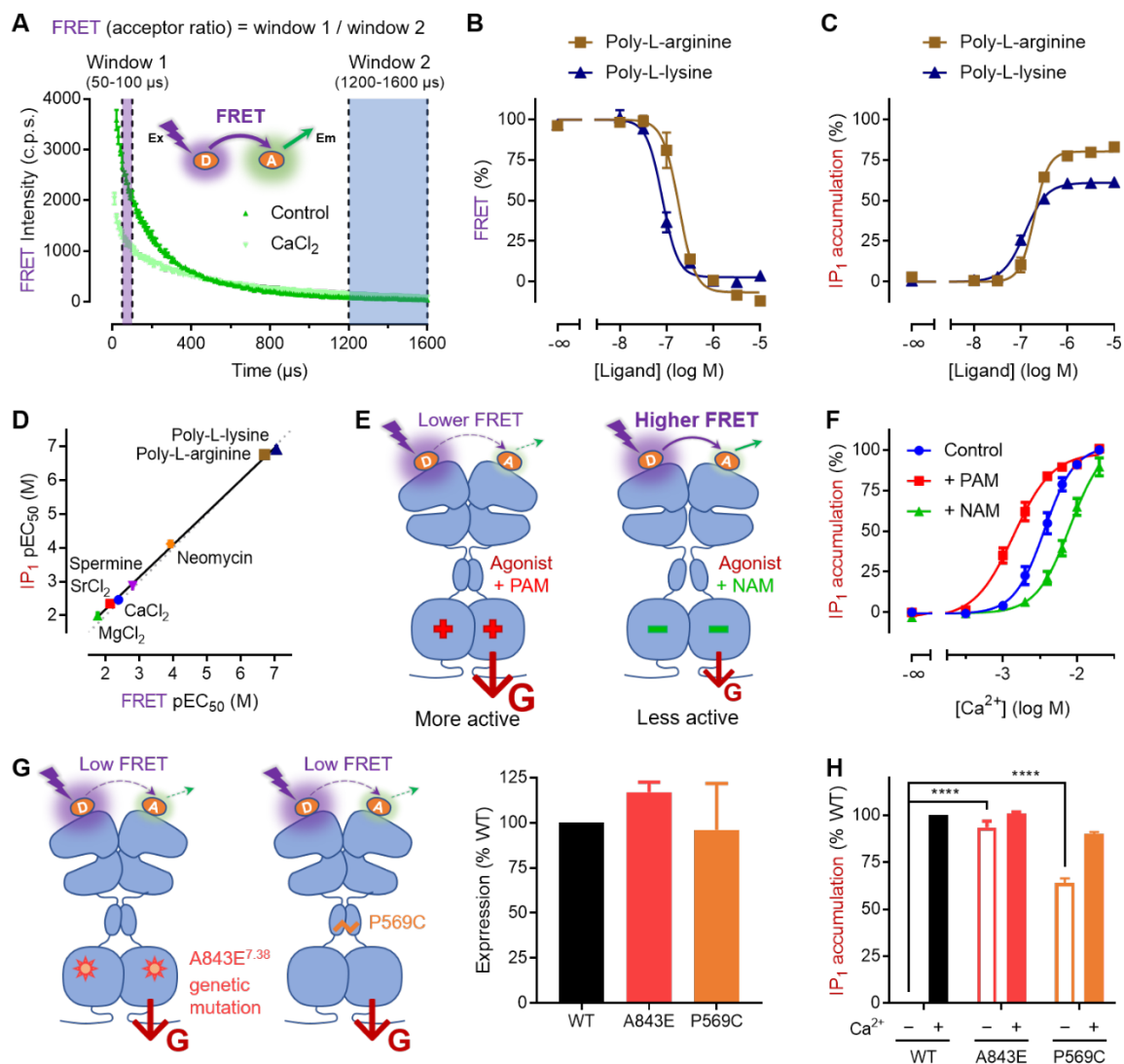
Supplementary Figures



Supplementary Figure 1. Monatomic ion binding sites in CaSR crystal structures. (A) Binding sites of the indicated monatomic ions in the different crystal ECD structures that were reported by two independent research groups (Geng *et al.*, *eLife*, 2016 and Zhang *et al.*, *Sci Adv*, 2016), in the active form 5K5S (CRD not shown), 5FBH and 5FBK, or in the resting form 5K5T biological assembly 2 (CRD not shown). (B) Cartoon illustrating these monatomic ion binding sites in the CaSR VFT dimer. From these structures, it is controversial whether site *b* and site *c* are binding sites for Ca²⁺ or Cl⁻.

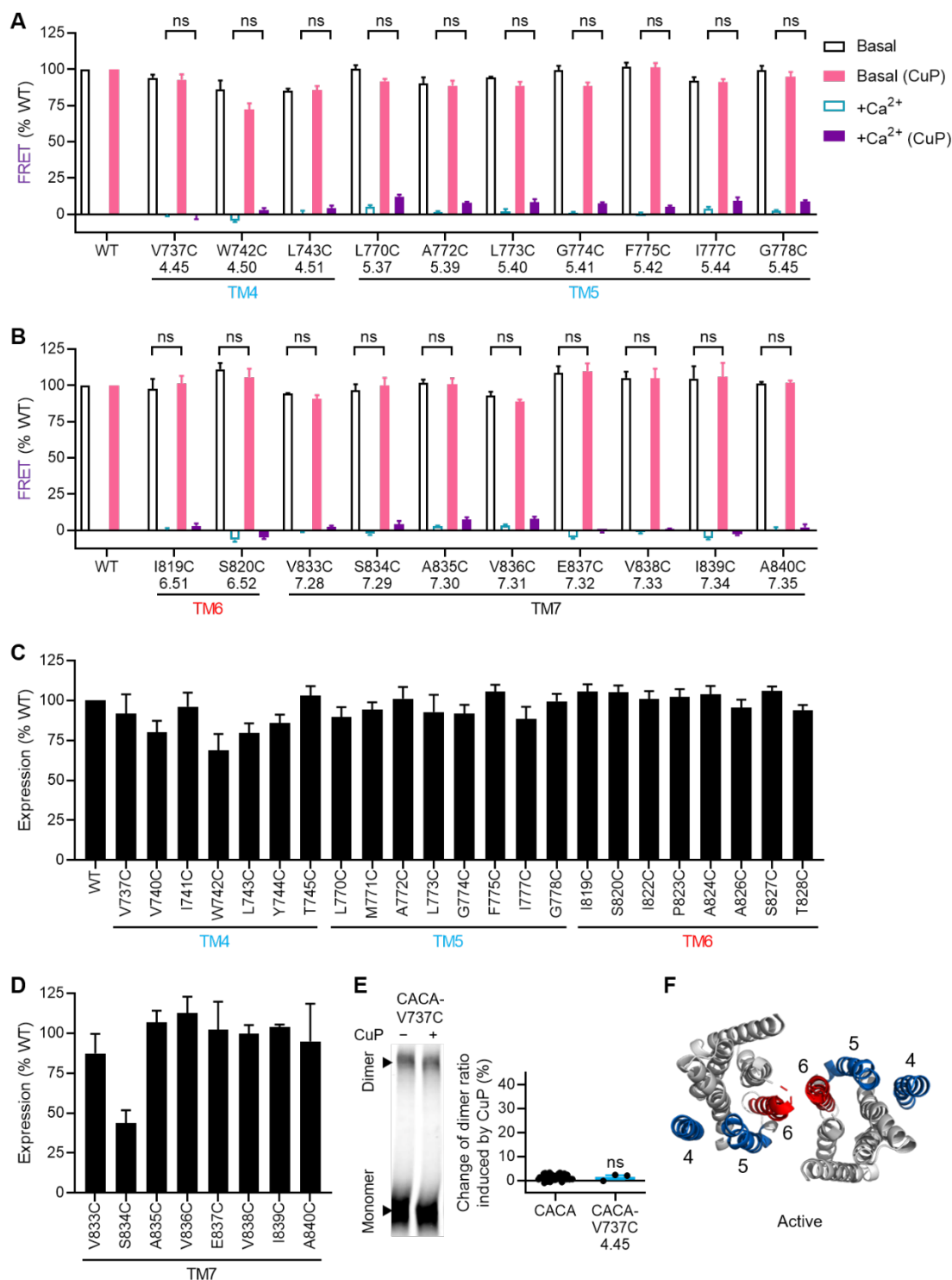


Supplementary Figure 2. Strategy to clarify nutrient effects on membrane receptors. Cartoon illustrating both the cell-based and the cell-free conditions used in this study to investigate the molecular basis of a pure nutrient action (x or y , as indicated) on a membrane receptor. The cell-free assay allows to measure the pure effect of a nutrient. It relies on the preparation of membrane extracts from cells expressing the receptor, and their extensive dialysis to discard all ambient nutrients. In contrast, cell-based assay responses may result from both the pure nutrient to be tested and the ambient ones.



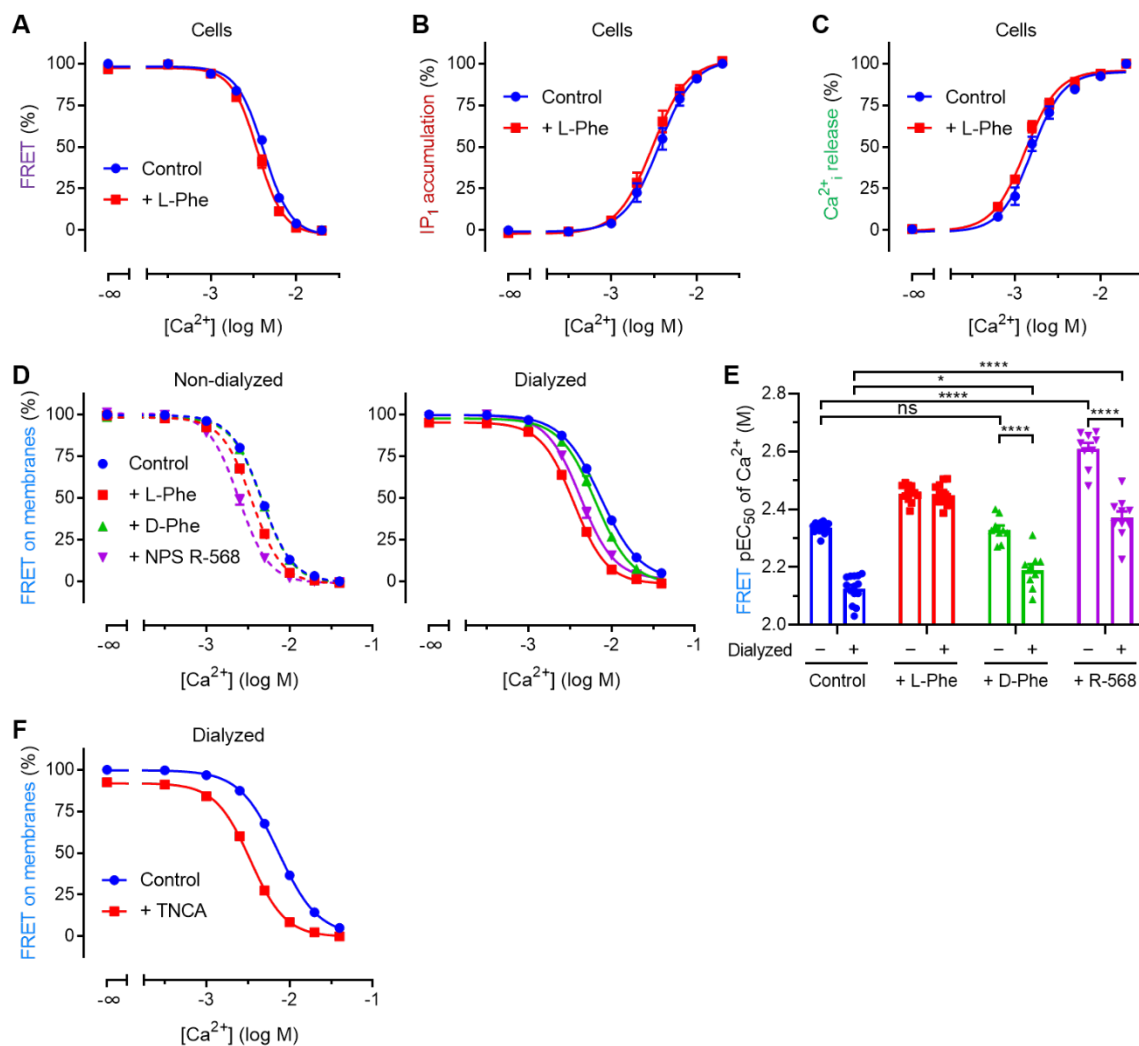
Supplementary Figure 3. Development of FRET sensor for CaSR. (A) Decays of FRET signal (acceptor emission after donor excitation) from the fluorescent-labeled CaSR dimer in the absence (dark green) or presence of 20 mM CaCl₂ (light green). The time windows of acceptor emission intensities used to calculate the FRET sensor values (acceptor ratio) are marked (window 1 in purple and window 2 in blue). Data are mean \pm SEM of a typical experiment performed in triplicates. (B-C) FRET sensor assay (B) and IP₁ accumulation assay (C) measured for poly-L-arginine and poly-L-lysine. Data are mean \pm SEM of at least three independent experiments performed in triplicates and normalized to the maximum response of CaCl₂. (D) Correlation between the potencies (pEC₅₀) of different agonists on CaSR determined by FRET sensor assay (X-axis) and IP₁ accumulation assay (Y-axis). Data are mean \pm SEM from the fitted curves for each individual experiment from at least three independent experiments. (E) Cartoon illustrating positive and negative allosteric modulators (PAM and NAM) that stabilize the active and resting conformation, respectively. (F) IP₁ accumulation measured for CaCl₂ in the presence of either PAM (10 μ M NPS R-568) or NAM (10 μ M NPS 2143). Data are mean \pm SEM of at least three independent experiments performed in triplicates and normalized to the maximum response of the control. (G) Cartoon illustrating the constitutive activation induced by the gain-of-function genetic mutation A843E^{7.38} in 7TM or the artificial cysteine cross-linking mutant P569C in CRD, and cell surface expression of the

indicated mutants measured by the emission of the fluorophore donor attached to the SNAP-tag. Data are mean \pm SEM of at least three independent experiments performed in triplicates and normalized to WT. **(H)** IP₁ accumulation measured for the mutants A843E or P569C in resting and active (20 mM CaCl₂) state (empty and filled, respectively). Data are mean \pm SEM of at least three independent experiments performed in triplicates and normalized to WT. Data are analyzed using two-way ANOVA with Tukey's multiple comparisons test to determine significance, with **** $P \leq 0.0001$.

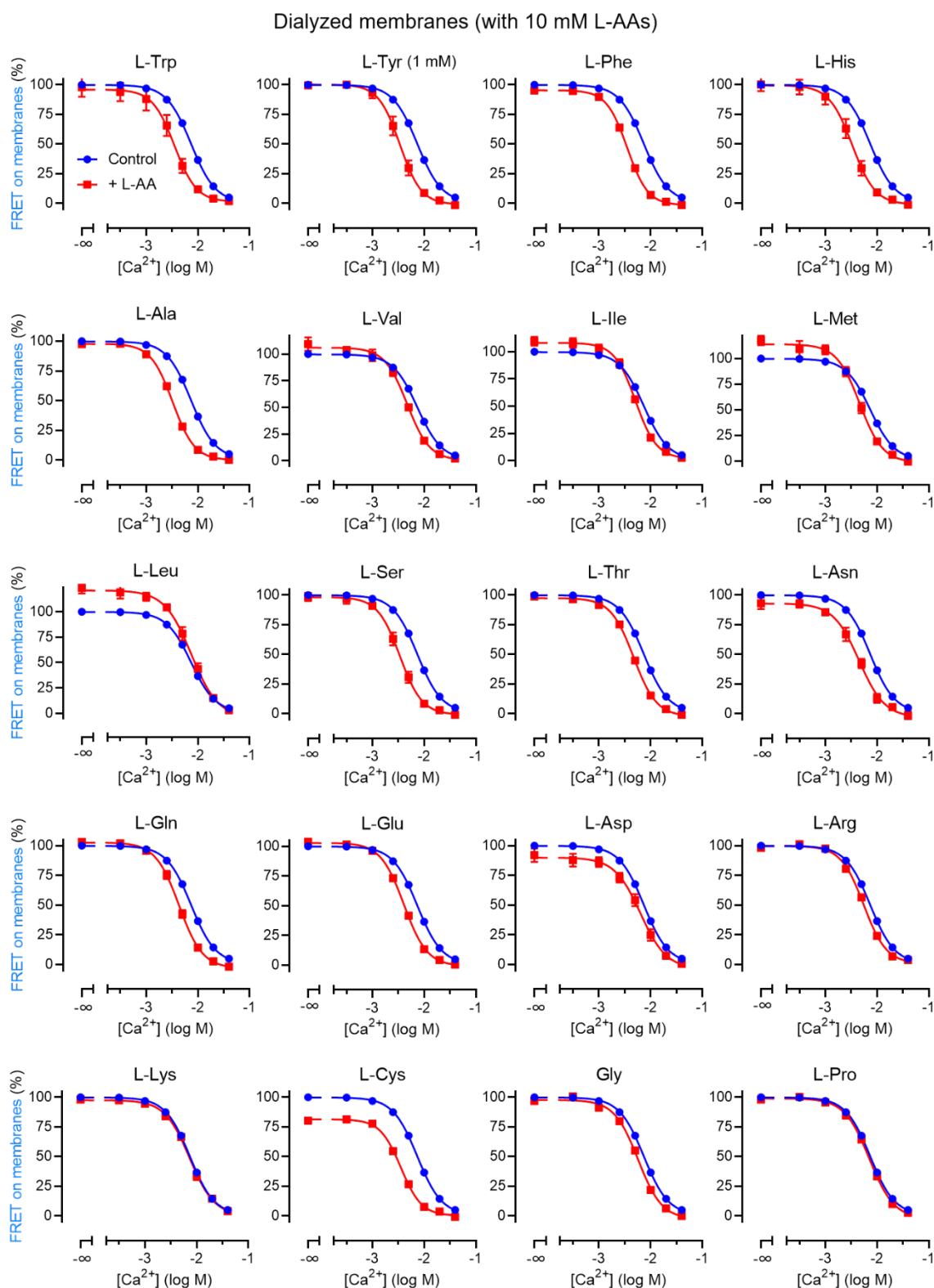


Supplementary Figure 4. Screening of CaSR 7TM interface by cysteine cross-linking. (A-B) Cysteine mutants screened by TR-FRET in the absence (black and pink) or presence of 20 mM CaCl₂ (blue and purple) with and without CuP treatment (filled and empty, respectively). Data are mean ± SEM of at least three independent experiments performed in triplicates and normalized to WT (data with and without CuP are normalized separately). Data are analyzed using two-way ANOVA with Tukey's multiple comparisons test to determine significance, with ns $P > 0.05$. **(C-D)** Cell surface expression of the indicated 7TM mutants by the emission of the fluorophore donor attached to the SNAP-tag. Data are mean ± SEM of at least three

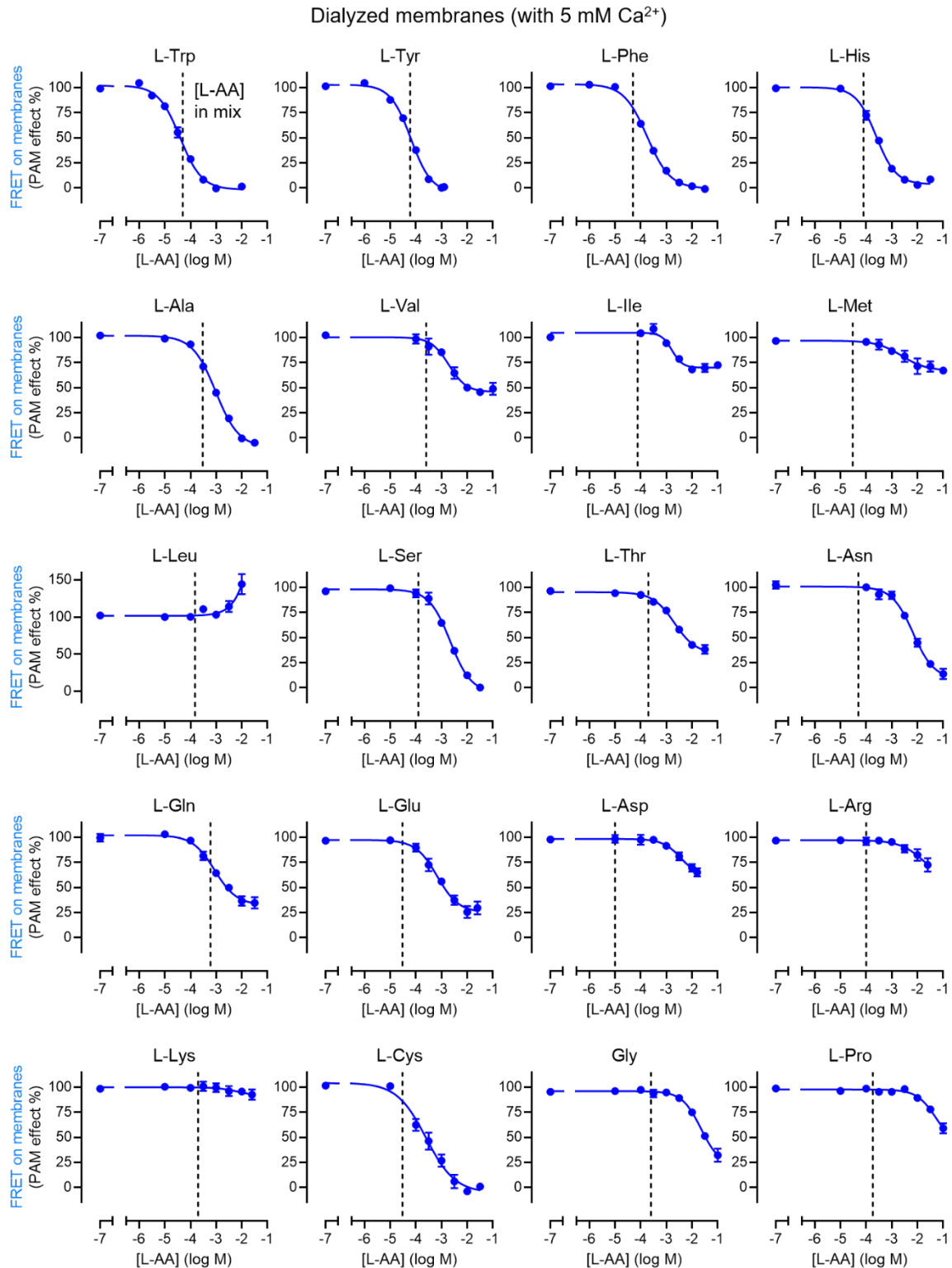
independent experiments performed in triplicates and normalized to WT. (E) Analysis of cell surface CaSR subunits of the indicated cysteine mutant in SDS-PAGE experiments under non-reducing conditions, after treatment (+) or without treatment (–) with CuP. Changes of dimer ratio induced by CuP treatment for this indicated mutant and the CACA control is quantified and shown. Quantitative data are mean \pm SEM of at least three independent experiments (n = 3 for CACA-V737C) while the blot is representative of one of these experiments. Data are analyzed using one-way ANOVA with Dunnett's multiple comparisons test to determine significance (compared with CACA control), with ns $P > 0.05$. (F) 3D model of the transmembrane domain interface of CaSR homodimer in the active state, where the TM6s are in direct contact.



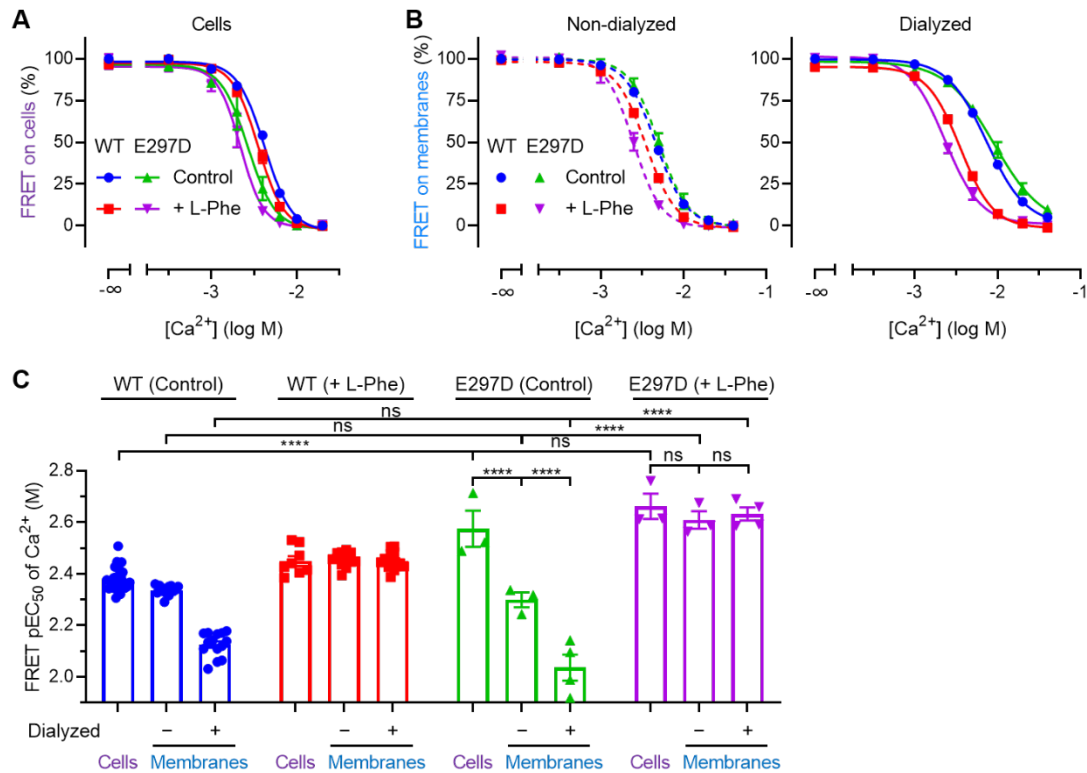
Supplementary Figure 5. Allosteric modulation of L-amino acids on CaSR in cells or membranes. (A-C) Effect of 10 mM L-Phe (red) in the cell-based FRET sensor assay (A), IP_1 accumulation assay (B) and intracellular calcium release assay (C), compared to the control conditions ($CaCl_2$ alone, blue). Data are mean \pm SEM of at least three independent experiments performed in triplicates and normalized to the control. (D) FRET measurement performed with $CaCl_2$ on non-dialyzed (dotted lines) and dialyzed (solid lines) membranes in the absence (as control, blue) or in the presence of 10 mM L-Phe (red), 10 mM D-Phe (green) or 10 μ M NPS R-568 (purple). Data are mean \pm SEM of at least three independent experiments performed in triplicates and normalized to the basal of control and the maximum response of L-Phe (non-dialyzed and dialyzed data are normalized separately). (E) FRET potencies (pEC₅₀) of calcium on non-dialyzed (-) or dialyzed (+) membranes in the absence (blue) or in the presence of 10 mM L-Phe (red), 10 mM D-Phe (green) or 10 μ M NPS R-568 (purple). Data are mean \pm SEM from at least eight independent experiments (n = 9-14). Two-way ANOVA with Tukey's multiple comparisons with **** $P \leq 0.0001$, * $P \leq 0.05$ and ns $P > 0.05$. (F) FRET measurement performed with $CaCl_2$ on dialyzed membranes in the absence (blue) or presence of 10 μ M TNCA (red). Data are mean \pm SEM of at least three independent experiments performed in triplicates and normalized to the basal of control and the maximum response of TNCA.



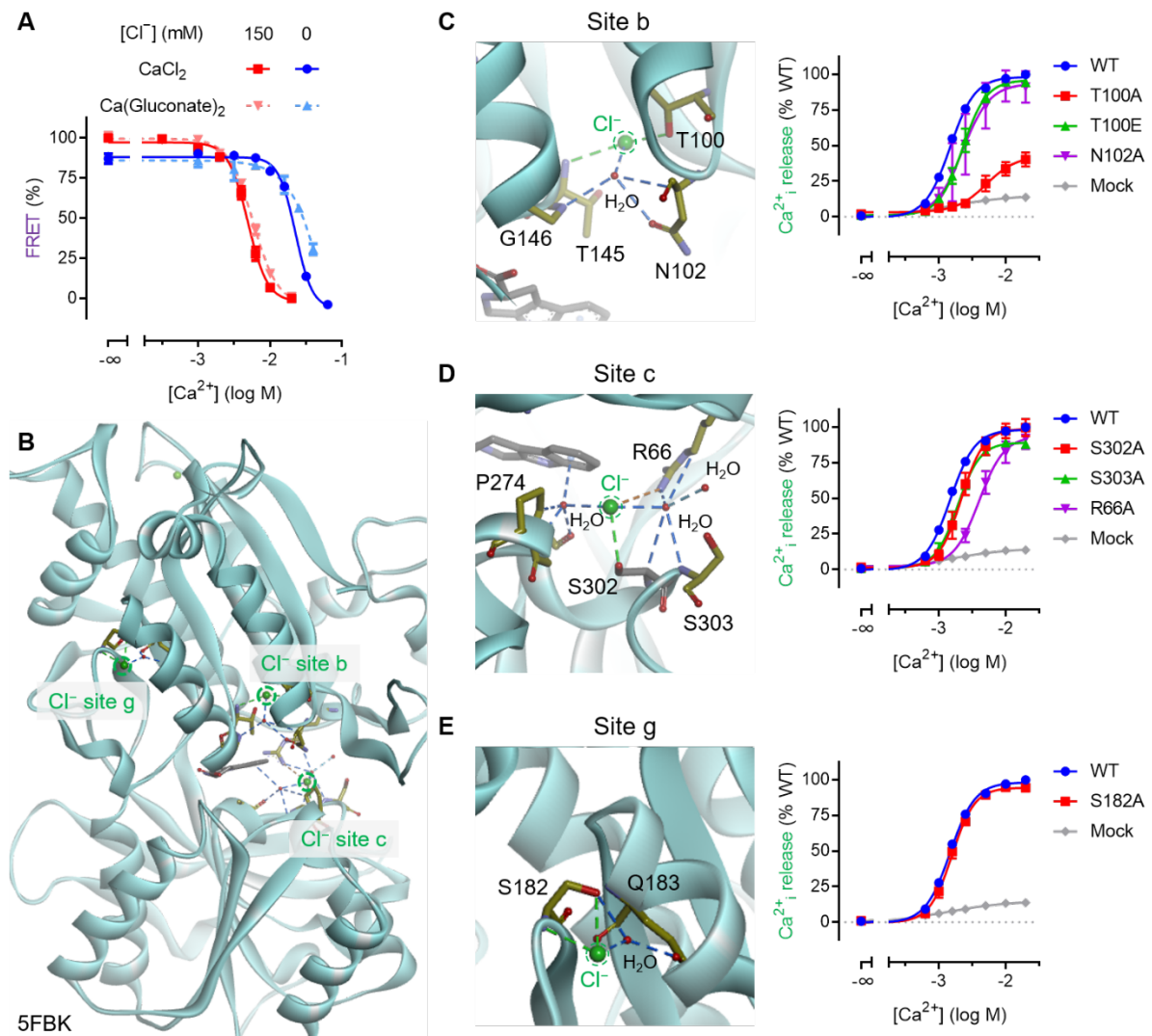
Supplementary Figure 6. Activation of CaSR by calcium ions is potentiated by L-AAs. FRET measurement performed with $CaCl_2$ on dialyzed membranes in the absence (blue) or presence of 10 mM L-AA (except 1 mM for L-Tyr). Data are mean \pm SEM of at least three independent experiments performed in triplicates and normalized to the basal of control and the maximum response of L-AA.



Supplementary Figure 7. Potency of the L-AAs on CaSR. FRET signal change induced by the indicated L-AA performed on dialyzed membranes in the presence of 5 mM CaCl₂. Data are mean ± SEM of at least three independent experiments performed in triplicates. Data are normalized to the basal conditions (5 mM CaCl₂ without L-AA) and the maximum response induced by L-AAs. The vertical dotted lines represent the related concentrations of L-AAs used in one-fold L-AA mixture (mimicking the conditions of fasting plasma as previously reported).



Supplementary Figure 8. Allosteric modulation of L-AA on CaSR with a genetic mutation E297D. (A) FRET measurements of CaSR with the genetic mutation E297D performed with CaCl₂ on cells in the absence (green) or presence of 10 mM L-Phe (purple). Data are mean \pm SEM of at least three independent experiments performed in triplicates and normalized to the control (CaCl₂ alone). (B) FRET measurements of the mutant E297D performed with CaCl₂ on non-dialyzed (dotted lines) and dialyzed (solid lines) membranes in the absence (green) or presence of 10 mM L-Phe (purple). Data are mean \pm SEM of at least three independent experiments performed in triplicates and normalized to the basal of control and the maximum response of L-Phe (non-dialyzed and dialyzed membrane are normalized separately). (C) FRET potencies (pEC₅₀) of calcium of CaSR WT or the mutant E297D on cells or non-dialyzed (-) or dialyzed (+) membranes in the absence (blue for WT, green for E297D) or presence of 10 mM L-Phe (red for WT, purple for E297D). Data are mean \pm SEM from at least three independent experiments ($n = 3-24$). Data are analyzed using two-way ANOVA with Tukey's multiple comparisons test, with **** $P \leq 0.0001$ and ns $P > 0.05$.



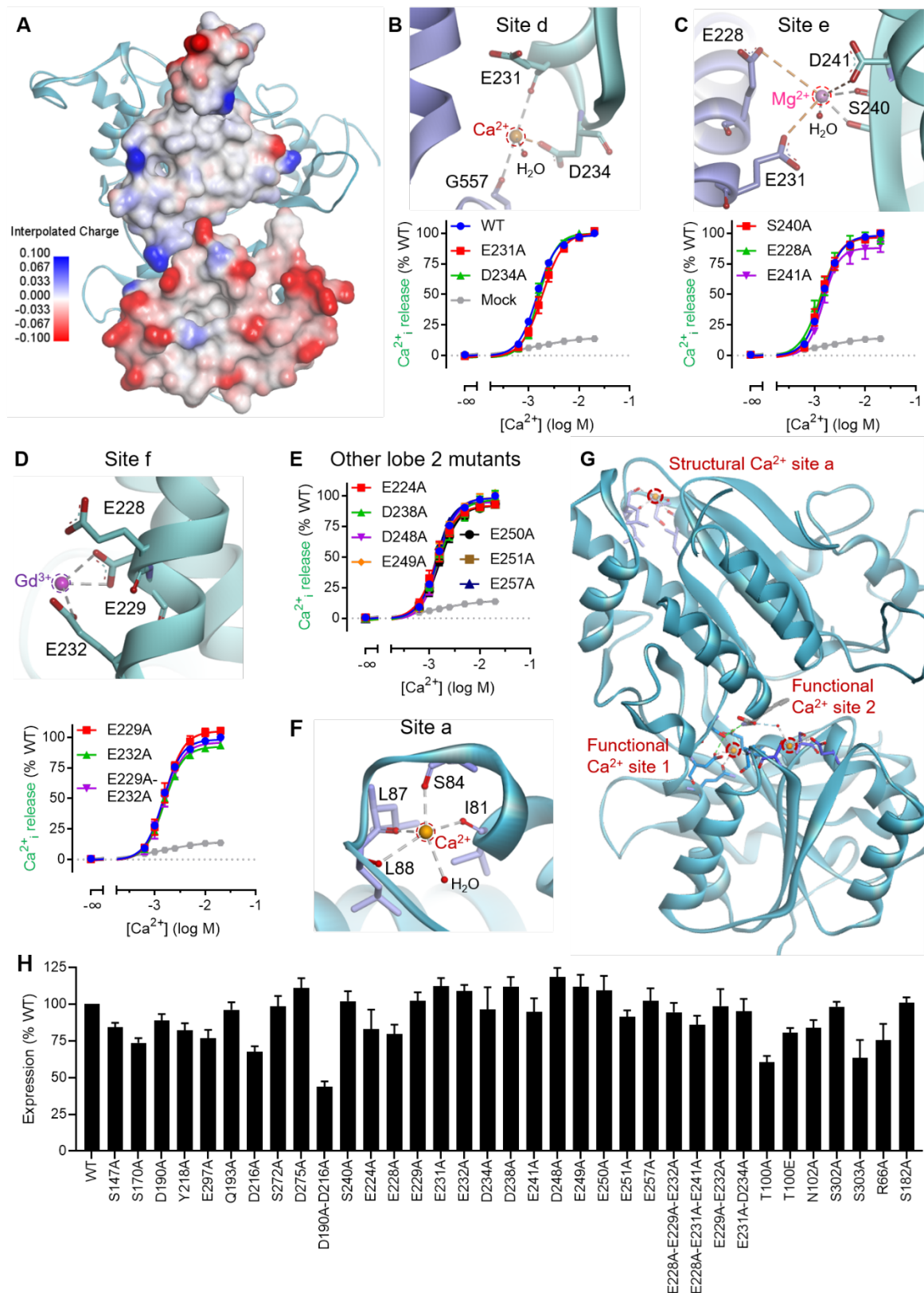
Supplementary Figure 9. Allosteric modulation and possible binding sites of chloride ions in CaSR VFT. (A) FRET measurement for calcium chloride (CaCl_2 , solid lines) or calcium gluconate (shown as $\text{Ca}(\text{Gluconate})_2$, dotted lines) performed in a buffer with no (0 mM Cl^- , blue) or high concentration of chloride ions (150 mM Cl^- , red). Data are mean \pm SEM of at least three independent experiments performed in triplicates and normalized to the maximum response of CaCl_2 in buffer with the high Cl^- concentration. (B) Three chloride binding sites (site *b*, *c* and *g*) were reported in the CaSR structure (PDB 5FBK). Sites *b* and *c* are in the VFT binding pocket. (C-E) Close-up view of chloride binding sites *b*, *c* and *g*, and intracellular calcium release for the indicated mutants in these sites. Data are mean \pm SEM of at least three independent experiments performed in triplicates and normalized to WT.

	66	100, 102	145, 147	170	190, 193	216, 218	272, 275	297	302
	Cl ⁻ site <i>b</i>			Ca ²⁺ site 1		Ca ²⁺ site 2		site <i>c</i>	
hCaSR	YNF ^R RGFR	IFD ^T CNTVS	VGAT ^G SSGV	YAS ^S SR	IPN ^D EHQATA	AADD ^D YGR	VFSS ^G PDLEP	LAS ^E AWAS ^S SLIA	
mVmn2r1	FNF ^R RGFR	IFD ^S CYTIS	VGSGG ^S SSL	YT ^S SCS	LPS ^D NLQSEA	AADD ^D YGR	LYTS ^D IDLSL	IAT ^E AWIT ^S ALIA	
zO1fCc1	FNF ^R AFR	IYD ^S CFTIS	VGAGG ^S SDL	YES ^S SCS	IPS ^D ENQ ^S VVA	AAED ^D YGR	VFSS ^D VDLSP	IASE ^E AWT ^S AAIS	
hGPRC6A	FEIS ^V FVL	IYD ^T CTEVT	IGSGY ^S EI	YES ^T AE	VPS ^D FHQ ^I KA	TTDD ^D YGR	VFLR ^Q FHVFD	IAS ^D NWST ^A TKIT	
zOR5.24	FYT ^K GLN	IYD ^T CSDVT	IGT ^S SSEI	YAS ^T TAT	VPS ^D DEY ^Q TCA	ITDGD ^D YGR	SFAK ^S SSQML	VAS ^D NWST ^A KHIL	
gOR5.24	YYT ^K GLN	IYD ^T CSDVT	IGP ^S SSSEI	YAS ^T TAT	VPN ^D EY ^Q THA	ITDGD ^D YGR	SFAK ^S SSQML	VAS ^D NWST ^S KNIL	
hT1R1	FNEH ^G YH	LYD ^V CSDSA	IGPD ^S STNR	YAS ^S SE	IPN ^D KY ^Q VET	GSS ^D DDYGR	VFSS ^R QLARV	VASE ^E AWAIST ^Y IT	
hT1R2	VKVIG ^Y N	IVD ^V CYISN	IGPD ^N SSES	YSA ^I SD	TPS ^A DHHIEA	VSS ^D TYGR	VFSP ^D LTLYH	IASE ^S WAID ^P VLH	
hT1R3	FSSN ^G LL	LFD ^T CSSEPV	IGPH ^S SSEL	YGA ^S ME	VPS ^D RV ^Q LTA	GSD ^D DEYGR	LFAS ^V HAAHA	VASE ^E AWLT ^S DLVM	
hmGluR1	REY ^Q GIQ	IRD ^S CWHSS	IGP ^G SSSV	YSA ^T SI	VPS ^D TL ^Q ARA	HTEG ^N YGE	CFCE ^G MTVRG	IGS ^D GWADR ^D EVI	
hmGluR5	REY ^Q GIQ	IRD ^S CW ^H SA	IGP ^G SSSV	YSA ^T SM	VPS ^D AA ^Q ARA	HTEG ^N YGE	CFCE ^G MTVRG	LGSD ^D GWADR ^D YDVT	
hmGluR2	NEHR ^G IQ	ILD ^S CSKDT	IGG ^S YS ^D V	YAS ^T SA	VPP ^D FF ^Q AKA	ASEG ^D YGE	LFTR ^S ED ^A RE	VAS ^D GWGA ^L ESVV	
hmGluR3	NED ^R GIQ	ILD ^T CSRDT	IGG ^S YS ^S V	YAS ^T SA	VPP ^D DF ^Y QAKA	ASEG ^D YGE	LFMR ^S DD ^S RE	VAS ^D GWGA ^Q ESII	
hmGluR4	KKE ^K GIH	ILD ^T CSRDT	IGAS ^G SSV	YAS ^T AP	VPS ^D TY ^Q AQA	ASEG ^S YGE	IFAN ^E DD ^I RR	MGSD ^S SWGSKI ^A PV	
hmGluR6	KKE ^Q GVH	LLD ^T CSRDT	VGAS ^A SSV	YAS ^T AP	VPP ^D SY ^Q AQA	ASEG ^N YGE	IFAN ^E DD ^I RR	VGS ^D SWGAK ^T SPI	
hmGluR7	KRENG ^I H	ILD ^T CSRDT	IGAS ^G SSV	YAS ^T AP	VPP ^D SF ^Q AQA	ASEG ^S YGE	IFAN ^E DD ^I KQ	VGS ^D SWGSKI ^N PL	
hmGluR8	KKE ^K GIH	ILD ^T CSRDT	IGAA ^A SSV	YAS ^T AP	VPP ^D SY ^Q AQA	ASEG ^N YGE	MFAN ^E DD ^I RR	IGSD ^S SWGSKI ^A PV	

Conserved for Cl⁻ binding in mGluRs

Conserved residues that interacts with the amino acid moiety of the various agonists

Supplementary Figure 10. Alignment of residues in the ion binding sites. The residues responsible for possible calcium binding sites 1 and 2 (red and orange, respectively), chloride binding site *b* (green) and ion binding site *c* (blue) of CaSR are aligned with other class C GPCRs. The purple boxes indicate the most conserved residues of the signature motif that interacts with the amino acid moiety, while the green box indicates the most conserved and important residue for chloride binding site in mGluRs.



Supplementary Figure 11. Possible calcium binding sites in CaSR VFT. (A) Electrostatic potential of VFT dimer interface (PDB 5FBK, side view). Lobe 2 interface contains several negative charged residues (Asp or Glu). (B-D) Close-up view of calcium binding sites *d* (PDB 5K5S), *e* (PDB 5FBH), and *f* (PDB 5FBH) in the lobe 2 interface, and intracellular calcium release for the indicated mutants in these sites. Data are mean \pm SEM of at least three

independent experiments performed in triplicates and normalized to WT. **(E)** Intracellular calcium release data of other indicated mutants for negative charged residues (Asp or Glu) in the lobe 2 interface. Data are mean \pm SEM of at least three independent experiments performed in triplicates and normalized to WT. **(F)** Close-up view of the structural calcium binding site *a* (PDB 5K5S). **(G)** 3D model of two possible functional sites *1* and *2* based on the crystal structure of the VFT (PDB 5K5S). The structural calcium binding site *a* is also shown. **(H)** Cell surface expression of mutants used for the monatomic ion binding sites by ELISA. Data are mean \pm SEM of at least three independent experiments performed in triplicates and normalized to WT.